NKG2A expression identifies a subset of human Vδ2 T cells exerting the highest antitumor effector functions

Valentina Cazzetta, Elena Bruni, Sara Terzoli, Claudia Carenza, Sara Franzese, Rocco Piazza, Paolo Marzano, Matteo Donadon, Guido Torzilli, Matteo Cimino, et al.

Cell Reports

Article

NKG2A expression identifies a subset of human Vδ2 T cells exerting the highest antitumor effector functions

Graphical abstract

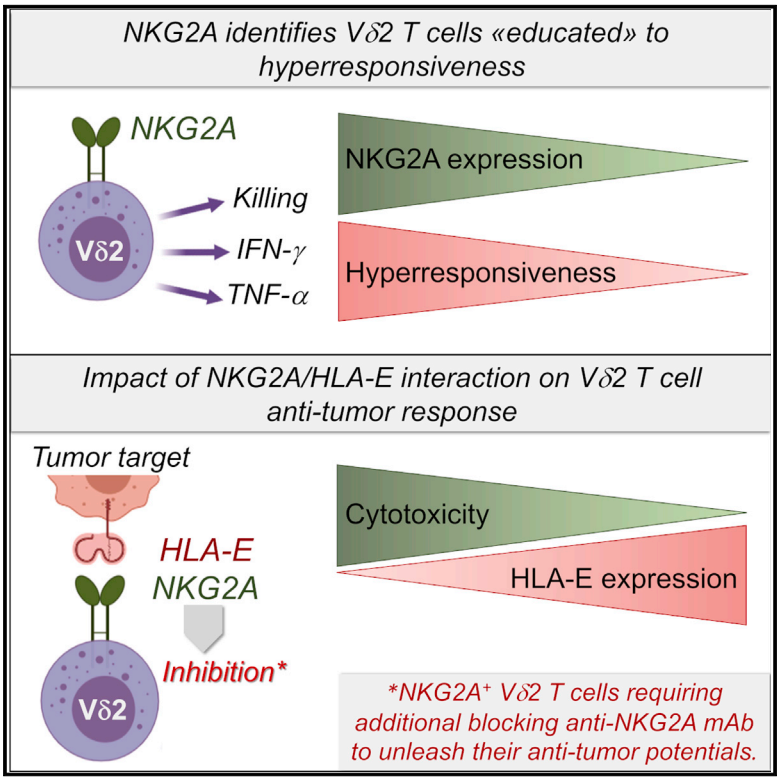

Highlights

- NKG2A identifies a Vδ2 T cell cluster "educated" to hyper-responsiveness against cancer
- Vδ2 T cell activation is finely tuned by NKG2A binding with HLA-E on cancer cells
- NKG2A$^+$ Vδ2 T cells are expandable *in vitro* from their precursors and are self-renewable
- Targeting NKG2A on Vδ2 T cells can prevent tumor escape from immune surveillance

Authors

Valentina Cazzetta, Elena Bruni, Sara Terzoli, ..., Silvia Della Bella, Joanna Mikulak, Domenico Mavilio

Correspondence

domenico.mavilio@unimi.it

In brief

Cazzetta et al. show that NKG2A expression identifies a subset of human self-renewable Vδ2 T cells "educated" to perform the highest effector functions in the clearance of cancer cells. The development of immunotherapy protocols targeting tumor-infiltrating NKG2A$^+$ Vδ2 T cells can be effective in improving patients' prognosis in several solid tumors.

Cazzetta et al., 2021, Cell Reports *37*, 109871
October 19, 2021
https://doi.org/10.1016/j.celrep.2021.109871

CellPress

Cell Reports

CellPress
OPEN ACCESS

Article

NKG2A expression identifies a subset of human Vδ2 T cells exerting the highest antitumor effector functions

Valentina Cazzetta,[1,2] Elena Bruni,[1,2] Sara Terzoli,[1] Claudia Carenza,[1,2] Sara Franzese,[1,2] Rocco Piazza,[3] Paolo Marzano,[1,2] Matteo Donadon,[4,5] Guido Torzilli,[4,5] Matteo Cimino,[5] Matteo Simonelli,[4,6] Lorenzo Bello,[7,8] Anna Villa,[9,10] Likai Tan,[11] Sarina Ravens,[11] Immo Prinz,[11] Domenico Supino,[12] Federico S. Colombo,[13] Enrico Lugli,[13,14] Emanuela Marcenaro,[15] Eric Vivier,[16,17,18] Silvia Della Bella,[1,2] Joanna Mikulak,[1,2,19] and Domenico Mavilio[1,2,19,20,*]

[1]Laboratory of Clinical and Experimental Immunology, IRCCS Humanitas Research Hospital, 20089 Rozzano, Milan, Italy
[2]Department of Medical Biotechnologies and Translational Medicine, University of Milan, Milan, Italy
[3]Department of Medicine and Surgery, University of Milan-Bicocca, Monza, Italy
[4]Department of Biomedical Science, Humanitas University, 20090 Pieve Emanuele, Milan, Italy
[5]Department of Hepatobiliary and General Surgery, IRCCS Humanitas Research Hospital, 20089 Rozzano, Milan, Italy
[6]Department of Medical Oncology and Hematology, IRCCS Humanitas Research Hospital, 20089 Rozzano, Milan, Italy
[7]U.O. Neurochirurgia Oncologica, IRCCS Istituto Ortopedico Galeazzi, Milan, Italy
[8]Department of Oncology and Hemato-Oncology, University of Milan, Milan, Italy
[9]Division of Regenerative, Medicine, Stem Cells and Gene Therapy, San Raffaele Telethon Institute for Gene Therapy, San Raffaele Scientific Institute, Milan, Italy
[10]Institute of Genetic and Biomedical Research, UOS Milan, National Research Council, Rozzano, Milan, Italy
[11]Institute of Immunology, Hannover Medical School, Hannover, Germany
[12]Department of Biomedical Science of Clinical and Experimental Immunology, Humanitas University, 20090 Pieve Emanuele, Milan, Italy
[13]Humanitas Flow Cytometry Core, IRCCS Humanitas Research Hospital, 20089 Rozzano, Milan, Italy
[14]Laboratory of Translational Immunology, IRCCS Humanitas Research Hospital, 20089 Rozzano, Milan, Italy
[15]Department of Experimental Medicine, Center of Excellence for Biomedical Research, University of Genoa, Genoa, Italy
[16]Aix Marseille University, CNRS, INSERM, CIML, Marseille, France
[17]Research Laboratories, Innate Pharma, Marseille, France
[18]Service d'Immunologie, Hôpital de la Timone, APHM, Marseille-Immunopôle, Marseille, France
[19]These authors contributed equally
[20]Lead contact
*Correspondence: domenico.mavilio@unimi.it
https://doi.org/10.1016/j.celrep.2021.109871

SUMMARY

Human Vδ2 cells are innate-like γδ T effectors performing potent immune surveillance against tumors. The constitutive expression of NKG2A identifies a subset of Vδ2 T cells licensed with an intrinsic hyper-responsiveness against cancer. Indeed, the transcriptomic profiles of NKG2A$^+$ and NKG2A$^-$ cells characterize two distinct "intralineages" of Vδ2 T lymphocytes that appear early during development, keep their phenotypes, and show self-renewal capabilities in adult life. The hyper-responsiveness of NKG2A$^+$ Vδ2 T cells is counterbalanced by the inhibitory signaling delivered by human leukocyte antigen E (HLA-E) expressed on malignant cells as a tumor-escape mechanism. However, either masking or knocking out NKG2A restores the capacity of Vδ2 T cells to exert the highest effector functions even against HLA-E$^+$ tumors. This is highly relevant in the clinic, as the different degrees of engagement of the NKG2A-HLA-E checkpoint in hepatocellular carcinoma, glioblastoma, and non-small cell lung cancer directly impact patients' overall survival. These findings open avenues for developing combined cellular and immunologic anticancer therapies.

INTRODUCTION

Unconventional γδ T cells are key players for tumor immune surveillance with promising roles in cancer immunotherapy (Sebestyen et al., 2020; Zou et al., 2017). These innate-like lymphocytes can recognize malignant cells through the engagement of several surface molecules, including γδ T cell receptors (γδTCRs), innate activating receptors (i.e., NKG2D), and natural cytotoxicity receptors (NCRs). The binding of these receptors with their tumor-associated ligands induces the secretion of cytotoxic granules (e.g., perforin and granzymes) and anti-cancer/proinflammatory cytokines (e.g., interferon [IFN]-γ and tumor necrosis factor [TNF]-α) (Hudspeth et al., 2012; Mikulak et al., 2019b; Vantourout and Hayday, 2013). In addition, γδ T cells modulate adaptive immune responses by priming αβ T cells, recruiting B cells, and activating dendritic cells (DCs)

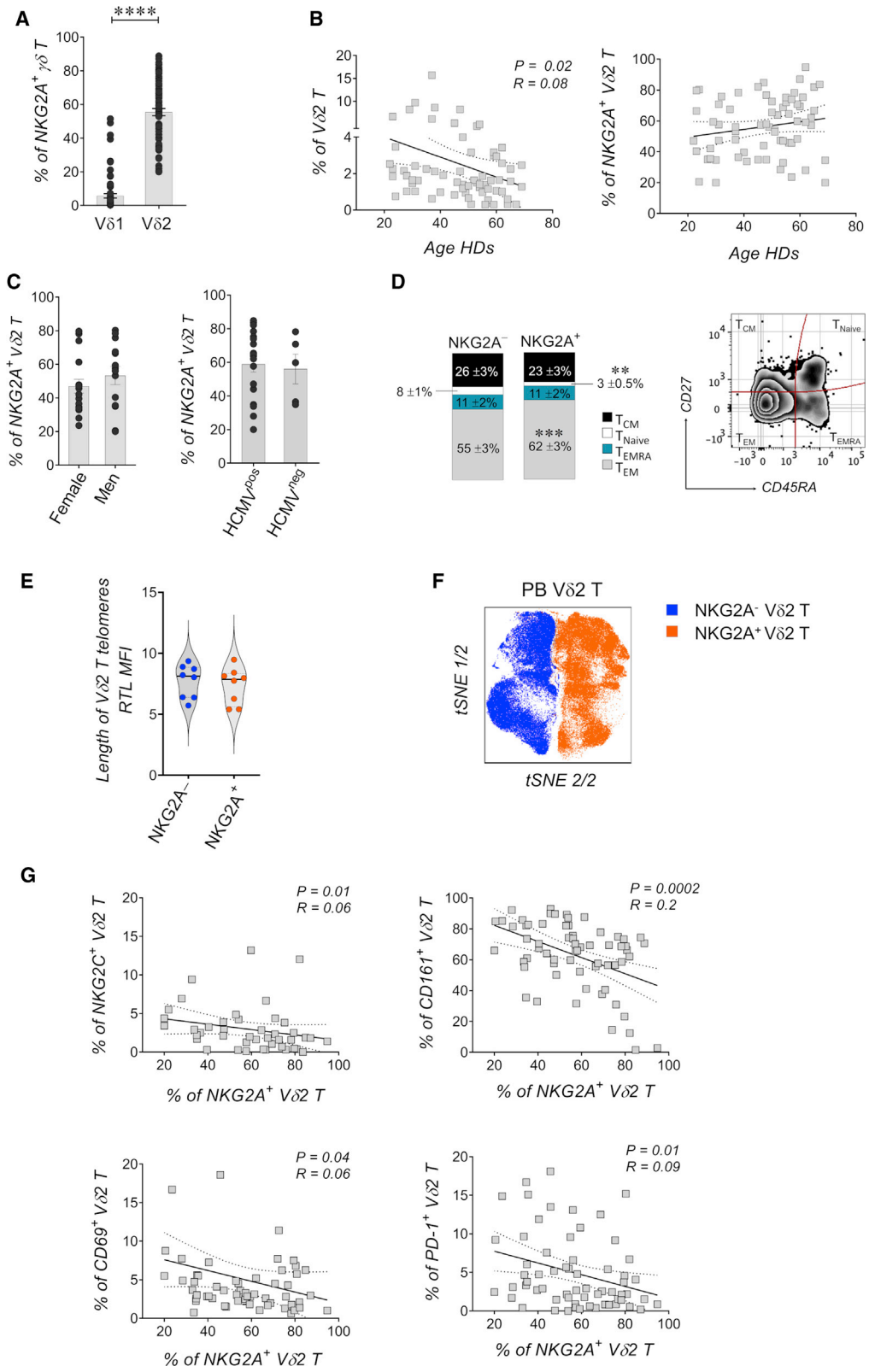

(legend on next page)

(Caccamo et al., 2006a; Ismaili et al., 2002; Wang et al., 2001). Human γδ T lymphocytes are divided into two main Vδ1 and Vδ2 subsets based on their TCRδ-chain expression (Vantourout and Hayday, 2013). While Vδ1 cells preferentially reside in peripheral tissues, Vδ2 T cells are mainly enriched in peripheral blood (PB) where they can reach 5% of all circulating T lymphocytes (Ribot et al., 2021). The direct activation of TCRs on Vδ2 cells in nonhuman/human primates but not in mice is induced by the specific recognition of phosphoantigens (PhAgs) that are intracellular metabolites of the mevalonate pathway highly produced by microbial-infected, stressed, or tumor-transformed cells (Eberl et al., 2003; Fichtner et al., 2020; Gober et al., 2003). This peculiar mechanism has been targeted to develop protocols of adoptive cell transfer therapies relying on the antitumor potentials of *in vitro/in vivo* expanded Vδ2 T cells (Godfrey et al., 2018). Although these approaches are safe, their overall antitumor efficacy is generally low and needs to be improved by selecting those Vδ2 T cell subsets exerting the highest effector functions against malignant cells.

NKG2A is an inhibitory receptor playing key roles in the differentiation, homeostasis, and functions of natural killer (NK), natural killer T (NKT), and $CD8^+$ αβ T cells (Mingari et al., 1998; Moretta et al., 1994; Zaghi et al., 2019). This lectin-type molecule pairs with CD94 to form a heterodimer that binds to the nonclassical class I human leukocyte antigen E (HLA-E) expressed on most human tissues (Kaiser et al., 2008; Taveirne et al., 2011). The inhibitory signal pathway of NKG2A relies on the engagement of intracytoplasmic immune-receptor tyrosine-based inhibition motifs (ITIMs) and of tyrosine phosphatases SHP-1 and SHP-2 (Joncker et al., 2009; Long et al., 2013). The overexpression of HLA-E in several tumor settings greatly limits the effector functions of tumor-infiltrating lymphocytes (TILs) through its binding with NKG2A. Indeed, the engagement of this inhibitory checkpoint makes it possible for malignant cells to escape from antitumor activities of $NKG2A^+$ TILs, thus greatly worsening the prognosis of different types of cancers (Abd Hamid et al., 2019; Bossard et al., 2012; Gooden et al., 2011; Wu et al., 2020). This rationale paved the way for the development of immunotherapies administering anti-NKG2A/CD94 monoclonal antibody (mAb) to unleash TIL effector functions (Andre et al., 2018; Mingari et al., 2019; van Hall et al., 2019; van Montfoort et al., 2018; Zaghi et al., 2019).

Growing evidence also highlighted the role of NKG2A in the so-called "education" of NK cells (He and Tian, 2017; Held, 2012). This process is finely tuned by the interactions of inhibitory receptors with their ligands to create unique cellular repertoires of immunological diversities that, in turn, confer variable reactivities and sensitivities to inhibition with the minimum number of encoded genes. These receptor-ligand interactions set the effector functions of NK cells at hyper-responsive levels in response to stimulatory activation. By contrast, NK cells that lack repressive signaling are rendered hyporesponsive (Boudreau and Hsu, 2018; He and Tian, 2017; Held, 2012; Yawata et al., 2008). While the education process was thought to control cell responsiveness primarily during cell development, experimental findings suggest that this phenomenon also occurs under disease conditions (Ivarsson et al., 2013). Although NKG2A is constitutively expressed at high levels on human Vδ2 T cells (Angelini et al., 2011; Pizzolato et al., 2019), its biological and functional relevance remains completely unexplored.

The present study demonstrates that expression of NKG2A identifies a subset of human Vδ2 T cells "educated" to perform the highest effector functions against cancer when compared to their $NKG2A^-$ counterpart. We also show here that both $NKG2A^+$ and $NKG2A^-$ Vδ2 T cells keep their distinct phenotype following activation/manipulation *in vitro* and are equipped with distinct self-renewal abilities starting from their thymocyte precursors, thus indicating the different intrinsic nature of these two subsets. Our results also support the paradigm whereby the supplied hyper-responsiveness of $NKG2A^+$ Vδ2 T cells is counterbalanced by the inhibitory signaling triggered by the binding of NKG2A to its ligand HLA-E. However, either the masking or knocking out of NKG2A restores the capacity of this Vδ2 T cell subset to exert its highest effector functions even against $HLA\text{-}E^+$ tumors. This is relevant in the context of several solid human tumors (e.g., hepatocellular carcinoma [HCC], glioblastoma [GBM], and non-small cell lung cancer [NSCLC]) in which the antitumor potential of cancer-infiltrating $NKG2A^+$ Vδ2 T cells is associated with different prognostic scores due to different degrees of HLA-E expression on malignant cells.

RESULTS

High expression of NKG2A identifies a distinct subset of PB Vδ2 T cells

We first performed an extensive multiparametric flow cytometry analysis to evaluate the distribution of NKG2A on total PB γδ T cells from healthy donors (HDs). Our results first confirmed that the expression of this receptor is mainly restricted to Vδ2 T cells (Figures 1A and S1A) (Angelini et al., 2011; Pizzolato

Figure 1. Phenotypic profile of peripheral blood $NKG2A^+$ Vδ2 T cells

(A–C) Statistical analysis of flow cytometry data showing NKG2A expression (% ± SEM) on Vδ2 and Vδ1 T cell subsets (n = 76) (A), Pearson's correlations between the percentage of the total (left) or $NKG2A^+$ (right) Vδ2 T cells and donor age (n = 67) (B), and frequency (% ± SEM) of $NKG2A^+$ Vδ2 T cells in age-matched (age ≤ 40 years) female (n = 17) and male (n = 14) donors (left) and in HCMV-negative (n = 5) and HCMV-positive (n = 19) individuals (right).

(D) Frequency (% ± SEM) of the T_{NAIVE}, T_{CM}, T_{EM}, and T_{EMRA} subpopulations in $NKG2A^+$ and $NKG2A^-$ Vδ2 T cells (n = 63; left), with one representative dot plot showing the differentiation status of PB Vδ2 T cells (right).

(E) Relative telomere length (RTL) calculated as the ratio of mean fluorescence intensity (MFI ± SEM) between the telomere-conjugated fluorescence of $NKG2A^+$ or $NKG2A^-$ Vδ2 T cells and the control 1301 cell line calculated with correction for the DNA index of $G_{0/1}$ cells.

(F) tSNE analysis of multiparametric flow cytometry data (Key Resources Table) performed on Vδ2 T cells (n = 26).

(G) Pearson's correlation between expression (%) of NKG2A and NKG2C, CD161, PD-1, and CD69 on Vδ2 T cells (n ≥ 43).

For the comparison of two groups of samples, the Kolmogorov-Smirnov test was applied. Experiments with more than two groups were analyzed by ANOVA with Tukey's comparison test. When specified, Pearson's rank correlations analysis was used. Statistical differences are represented as p values: $^{**}p < 0.01$; $^{***}p < 0.001$; $^{****}p < 0.0001$.

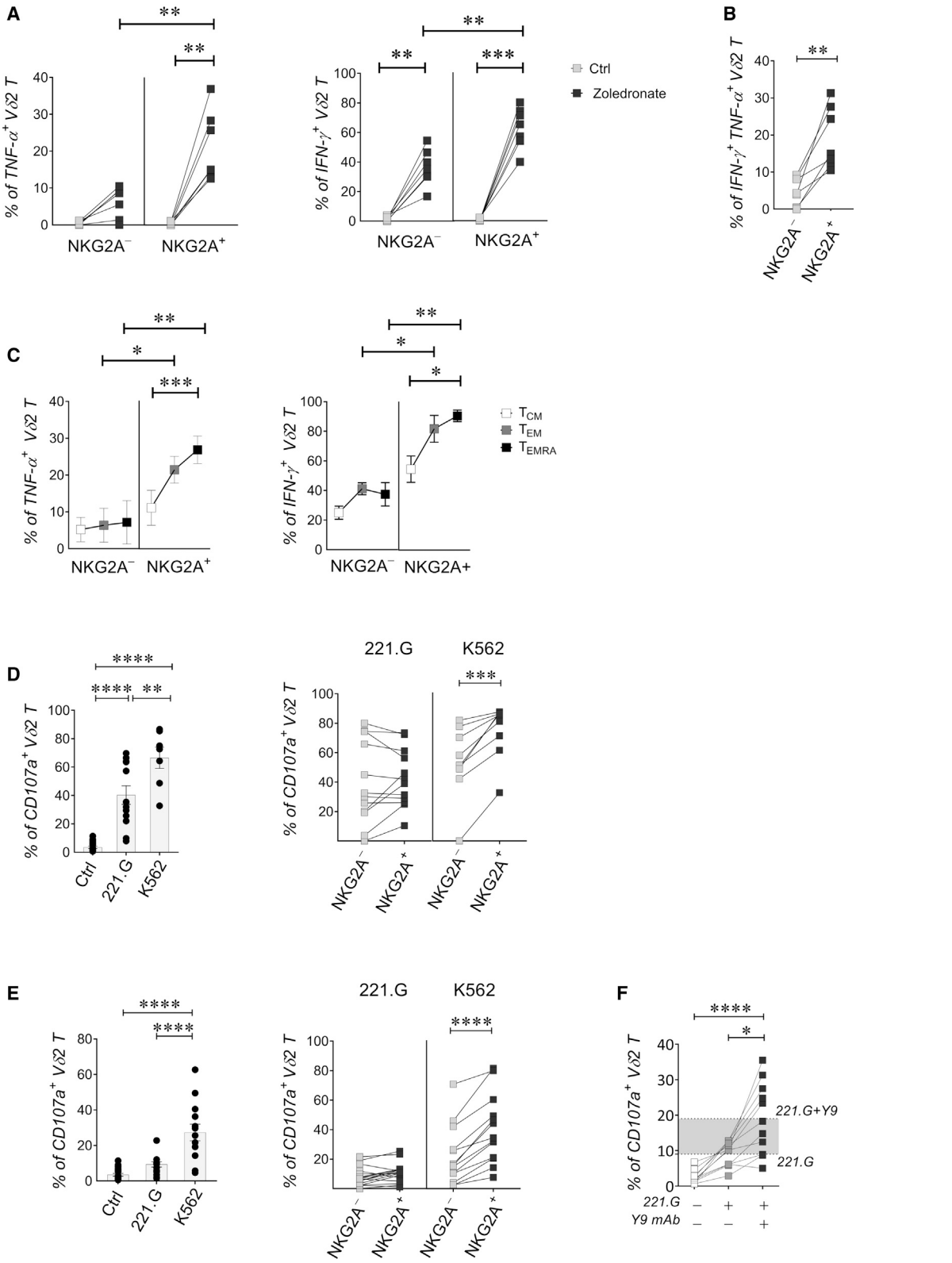

(legend on next page)

et al., 2019). Although the frequency of total PB Vδ2 T cells had been reported to decline with aging (Bruni et al., 2019; Caccamo et al., 2006b), we observed that the percentage of NKG2A$^+$ Vδ2 T cells remains stable in the PB regardless of the age and sex of the HDs. Not even the presence of human cytomegalovirus (HCMV) infection, a pathogen known to drive γδ T cell differentiation (Davey et al., 2018; Mikulak et al., 2019a), affected the expression of NKG2A on Vδ2 T cells (Figures 1B and 1C).

We then assessed the differentiation pattern of NKG2A$^+$ and NKG2A$^-$ Vδ2 T cells in accordance with their expression of CD27 and CD45RA (Bruni et al., 2019; Caccamo et al., 2005). Our data showed that T effector memory (T_{EM}) cells (CD27$^-$CD45RA$^-$) represent the largest fractions within both subsets, although NKG2A$^+$ Vδ2 T cells comprise significantly higher frequencies of T_{EM}s compared to their NKG2A$^-$ counterparts. Both NKG2A$^+$ and NKG2A$^-$ Vδ2 T cells showed similar frequencies of T central memory (T_{CM}) cells (CD27$^+$CD45RA$^-$) and highly differentiated effector memory (T_{EMRA}) cells CD27$^-$CD45RA$^+$, while T naïve (T_{Naive}) cells (CD27$^+$CD45RA$^+$) are more represented in the NKG2A$^-$ Vδ2 T cell compartments compared with their NKG2A$^+$ counterparts (Figure 1D). We also found that circulating NKG2A$^+$ and NKG2A$^-$ Vδ2 T cells undergo similar telomere shortening, thus indicating that both subsets have similar lifespans in PB (Figure 1E). Unbiased t-distributed stochastic neighbor embedding (tSNE) analysis adopted to multiparametric flow cytometry data revealed that the expression of NKG2A identifies two distinct and phenotypically different Vδ2 T populations (Figure 1F). In particular, we observed that NKG2A expression on Vδ2 T cells inversely correlates with surface levels of the activating receptors CD69 and NKG2C that, similar to NKG2A, pairs with CD94 to bind HLA-E ligand (Hudspeth et al., 2013). NKG2A also negatively correlates with CD161, whose expression is associated with a higher T and NK cell responsiveness to cytokine-driven activation (Kurioka et al., 2018). Finally, we found that lower expression of NKG2A pairs with higher surface levels of the checkpoint inhibitor and T cell exhaustion marker PD-1 (Blank et al., 2019). However, we did not find any significant correlation between the surface levels of NKG2A on Vδ2 T cells and the expressions of NKG2D or CD56, two markers associated with γδ T cell antitumor activities (Correia et al., 2013; Lee et al., 2020) (Figures 1G, S1B, and S1C).

NKG2A$^+$ Vδ2 T cells are endowed with the highest effector functions upon activation *in vitro*

We then evaluated whether the expression of NKG2A has any significant impact on the effector functions of Vδ2 T cells following stimulation *in vitro*. To this end, freshly purified peripheral blood mononuclear cells (PBMCs) were incubated with zoledronate to induce the secretion of PhAgs, which, in turn, activate Vδ2 T cells through the direct engagement of γδTCR (Eberl et al., 2003; Sebestyen et al., 2020). Surprisingly, we observed that NKG2A$^+$ Vδ2 T cells produce significantly higher amounts of TNF-α and IFN-γ upon γδTCR stimulation. Even the frequencies of Vδ2 T cells simultaneously producing IFN-γ and TNF-α are much higher in the NKG2A$^+$ compartment compared to the NKG2A$^-$ one (Figures 2A and 2B). The decreased ability of NKG2A$^-$ Vδ2 T cells to synthetize these two antitumor and proinflammatory cytokines is not associated with a zoledronate-induced apoptosis, as the frequencies of Annexin-V$^+$ Vδ2 T cells were similar in both NKG2A$^+$ and NKG2A$^-$ populations (Figure S2A). We also observed that the higher capacity to produce IFN-γ and TNF-α is maintained in all effector compartments (i.e., T_{EM} and T_{EMRA}) of NKG2A$^+$ Vδ2 T cells when compared with their NKG2A$^-$ counterparts (Figure 2C). These findings clearly indicate that the hyper-responsiveness of NKG2A$^+$ Vδ2 T cells is not due to their higher frequencies in the T_{EM} subpopulation (Figure 1D), but rather it is associated with their intrinsic higher capacity to respond upon PhAg stimulation. Because of the reported ability of Vδ2 T cells to produce interleukin (IL)-17A (Caccamo et al., 2011), we also assessed the production of this proinflammatory cytokine upon zoledronate treatment but did not find any differences in its production between NKG2A$^+$ and NKG2A$^-$ Vδ2 T cells (Figure S2B).

We then performed a sensitive CD107a degranulation flow-cytometry-based assay to evaluate the cytotoxic potentials of both NKG2A$^+$ and NKG2A$^-$ Vδ2 T cells following incubation with several tumor cell targets (Lorenzo-Herrero et al., 2019). To do so, Vδ2 T cells were cocultured with either HLA-E$^-$ K562 cells or HLA-E$^+$ 721.221.G (221.G) cells previously primed with zoledronate to release PhAgs (Figure S2C) (Roberto et al., 2018). We first observed that the percentages of total CD107$^+$ Vδ2 T cells significantly increased in the presence of both tumor cell targets and reached the highest frequencies with K562 (Figure 2D). Notably, the CD107a degranulation level of NKG2A$^+$ and

Figure 2. Impact of NKG2A on effector functions of peripheral blood Vδ2 T cells

(A) Statistical analysis of flow cytometry data showing frequencies (%) of TNF-α (left) or IFN-γ (right) production (%) from NKG2A$^+$ and NKG2A$^-$ Vδ2 T cells either in the absence (Ctrl) or in the presence of stimulation *in vitro* with zoledronate (n = 7).

(B) Statistical analysis of flow cytometry data showing frequencies (%) of NKG2A$^+$ and NKG2A$^-$ Vδ2 T cells producing TNF-α and IFN-γ cytokines following stimulation *in vitro* with zoledronate (n = 7).

(C) Statistical analysis of flow cytometry data showing frequencies (% ± SEM) of NKG2A$^+$ and NKG2A$^-$ Vδ2 T_{CM}, T_{EM}, and T_{EMRA} subsets producing TNF-α (left) or IFN-γ (right) following stimulation *in vitro* with zoledronate.

(D) Statistical analysis of flow cytometry data showing frequencies (% ± SEM) of CD107a$^+$ total Vδ2 T cells (left) and of CD107a$^+$ NKG2A$^+$ (gray squares) and NKG2A$^-$ (black squares) Vδ2 T cells (right) either in the absence (Ctrl in left) or in the presence of 221.G and K562 prestimulated with zoledronate (n ≥ 9).

(E) Statistical analysis of flow cytometry data showing frequencies (% ± SEM) of CD107a$^+$ total Vδ2 T cells (left) and of CD107a$^+$ NKG2A$^+$ (gray squares) and NKG2A$^-$ (black squares) Vδ2 T cells (right) either in the absence (Ctrl in left) or in the presence of 221.G and K562 without zoledronate stimulation (n ≥ 13).

(F) Statistical analysis of flow cytometry data showing frequencies (%) of CD107a$^+$ Vδ2 T cells either in the absence (Ctrl in white squares) or in the presence 221.G cell alone (gray squares) or preincubated with anti-NKG2A/CD94-blocking mAb/Y9 (black squares) (n = 11). The gray area represents the mean difference in CD107a expression between 221.G alone and mAb/Y9+221.G-treated samples.

For the comparison of two groups of samples t test was applied. Experiments with more than two groups were analyzed by ANOVA test with Tukey's comparison test. Statistical differences are represented as p values: *p < 0.05; **p < 0.01; ***p < 0.001; ****p < 0.0001.

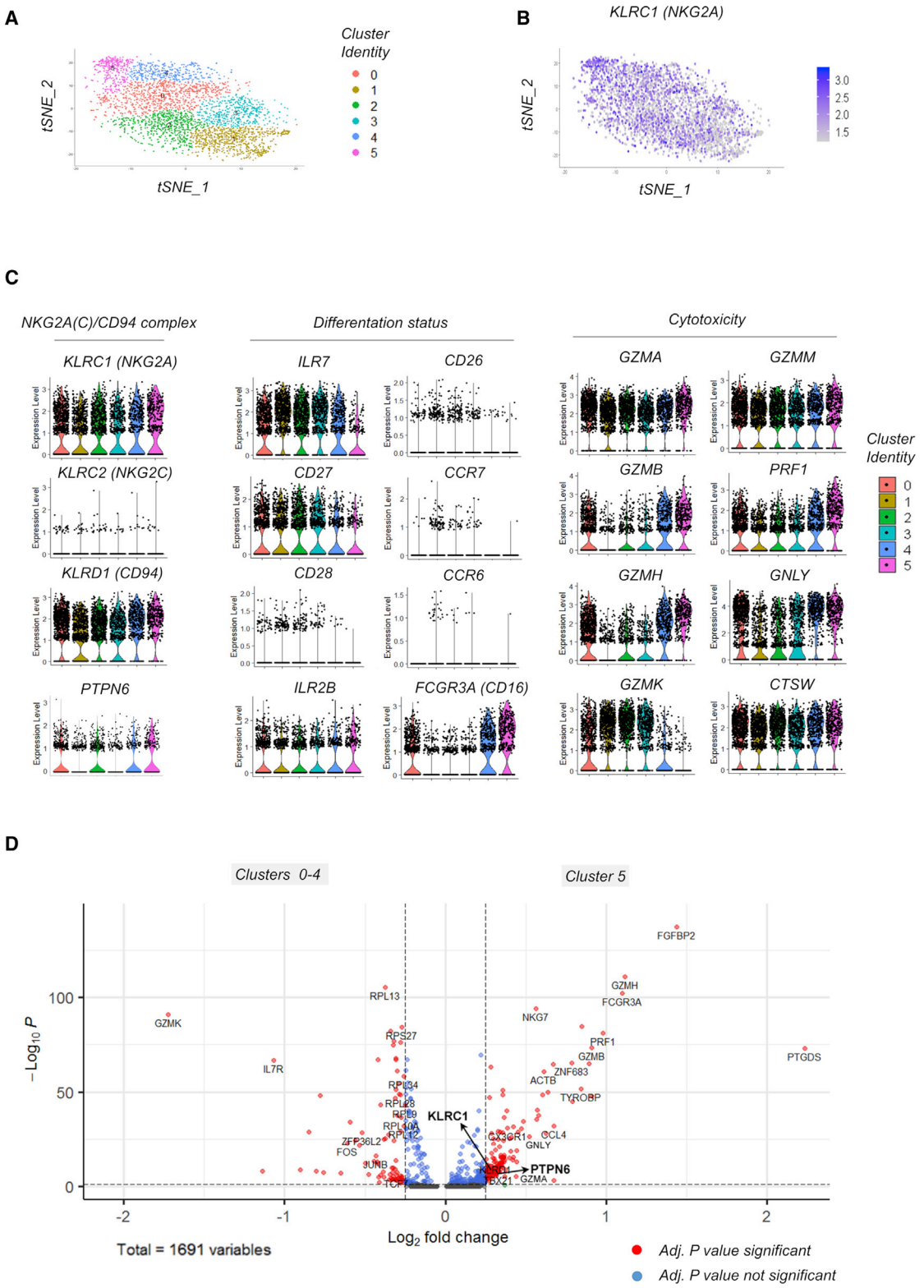

Figure 3. scRNA-seq analysis of peripheral blood Vδ2 T cells

(A) tSNE plot of total Vδ2 T cell clusters (c0–c5) (n = 3; GEO: GSE128223).

(B) *NKG2A* gene projection on the tSNE plot of total Vδ2 T cells.

(legend continued on next page)

NKG2A$^-$ Vδ2 T cells appeared similar against 221.G, while NKG2A$^+$ Vδ2 T cells showed a significantly higher capacity to express CD107a against K562 compared to their NKG2A$^-$ counterparts. Human γδ T cells can also exert their cytotoxic potential through the direct engagement of innate activating receptors such as NKG2D or NCRs and without the release of PhAgs (Hudspeth et al., 2013; Vantourout and Hayday, 2013). Hence, we also tested the cytotoxic potential of Vδ2 T cells in the absence of incubation with zoledronate. Incubation with K562 alone significantly increased the frequencies of CD107a$^+$ Vδ2 T cells (Figure 2E), although at lower levels compared to the experimental results shown in Figure 2D. Again, NKG2A$^+$ Vδ2 T cells showed a significantly higher capacity to degranulate against K562 compared with their NKG2A$^-$ counterparts even in the absence of a direct stimulation of γδTCR by PhAgs. In contrast, incubation of nonstimulated Vδ2 T cells with 221.G failed to trigger the expression of CD107a, independently from NKG2A expression. As expected, the degranulation capacity of both NKG2A$^+$ and NKG2A$^-$ Vδ2 T cells correlates with their direct effective killing of tumor K562 target cells, although lower lytic activity was found for NKG2A$^-$ compared to NKG2A$^+$ Vδ2 T cells (Figure S2D).

These experimental findings suggest that the presence of HLA-E on the tumor target plays a key role in reducing Vδ2 T cell cytotoxicity through its binding with the inhibitory checkpoint NKG2A. To confirm this working hypothesis, we incubated freshly purified Vδ2 T cells with 221.G in either the presence or absence of a blocking antibody (Y9) against the CD94/NKG2A heterodimer and without incubation with zoledronate. Notably, the masking of NKG2A significantly increased the ability of Vδ2 T cells to degranulate even against HLA-E$^+$ 221.G (Figure 2F). Hence, the intrinsic hyper-responsiveness of NKG2A$^+$ Vδ2 T cells against cancer cells is counterbalanced by the inhibitory signaling delivered by NKG2A following its binding with HLA-E as a mechanism of tumor escape.

The hyper-responsiveness of NKG2A$^+$ Vδ2 T cells is associated with a distinct transcriptional profile

To further investigate the intrinsic features of NKG2A$^+$ Vδ2 T cells, we analyzed single-cell (sc) RNA-seq data generated from PB Vδ2 T cells isolated from HDs (Pizzolato et al., 2019). Principal component analyses (PCAs) followed by tSNE analysis revealed six different Vδ2 T cell clusters showing distinct transcriptional profiles (c0–c5) (Figures 3A and S3). The expression of *KLRC1*, the gene encoding for NKG2A, was investigated in all Vδ2 T cell clusters together with the transcripts associated with differentiation and activation cellular status (Figures 3B and 3C). Clusters c1–c3 comprise less mature Vδ2 T cells, as indicated by their higher levels of *CD28*, *ILR7*, *CCR7*, *CCR6*, and *CD26* and lower expressions of *CD27*, *ILR2B*, and *FCGR3A* (*CD16*) (Figure 3C) (Bruni et al., 2019). We also analyzed the expression levels of several cytotoxic molecules including granzymes (*GZMA*, *GZMB*, *GZMH*, *GZMM*, and *GZMK*) and pore-forming molecules such as perforin (*PRF1*) and granulysin (*GNLY*), all of which are able to induce the death of target cells (Bovenschen and Kummer, 2010; Kishi et al., 2002). Predictably, these cells are characterized by lower levels of cytotoxic molecules such as *GZMB*, *GZMH*, *PRF1*, and *GNLY*. In contrast, the CD27^{low} clusters (c0, c4, c5) depict Vδ2 T$_{EM}$ cells showing high expression of cytotoxic factors (*GZMB*, *GZMH*, *PRF1*, *GNLY*) together with increased levels of *FCGR3A* and *ILR2B*. In accordance, CD27^{low} Vδ2 T$_{EM}$ cell clusters are characterized by the down modulation of *CCR7*, *CCR6*, and *ILR7*. Of note, high levels of *KLRC1* and *KLRD1* (transcripts encoding for NKG2A and CD94, respectively) were observed in all Vδ2 T cell clusters independently from their differentiation stages, although we found the highest level of *KLRC1* expression in c5 (Figures 3C and 3D). By contrast, *KLRC2*, the transcript encoding for NKG2C, is expressed at low levels in all Vδ2 T cell clusters. These transcriptomic profiles recapitulate our flow cytometry data showing high expressions of NKG2A/*KLRC1* on all Vδ2 T cell subsets regardless of their maturation stages (Figures 1D and 3C). In addition, *PTPN6*, the gene encoding for SHP1 and crucial for tuning NK cell education (Kabat et al., 2002; Viant et al., 2014), is also expressed at higher levels in c5 compared to the other clusters. In this regard, the analysis of differentially expressed genes (DEGs) between c5 and all other Vδ2 T cell clusters (c0–c4) confirmed our functional data. *De facto*, c5 is equipped with a strong inhibitory transcriptome associated with the highest expression of *NKG2A*, *CD94*, and *SHP1*, while achieving the maximal functional plasticity as indicated by the highest transcript levels of cytotoxic molecules (i.e., *PRF1*, *GZMA*, *GZMB*, *GZMH*, and *GNLY*) (Figure 3D). Moreover, cells comprised in c5 are also characterized by the lowest expression of several ribosomal proteins (e.g., *RPL12-14* or *RPS27*), thus suggesting their stable transcriptional profile with a limited protein turnover.

We then performed pseudotime analyses associated with the expression of *NKG2A.* These data revealed two main trajectories (S2 versus S0) referred to a gradual maturation of Vδ2 T cells. Interestingly, S0 and S2 branches are characterized by different effector-function potentials, with the S0 trajectory being more highly enriched with c5, the cluster equipped with the strongest cytotoxicity. Indeed, density plots clearly showed that the highest expression of *KLRC1* at the end of S0 trajectory matches the highest transcript levels of *IFN-γ* and Lysosomal Associated Membrane Protein 1 (*LAMP1)* (Figures 4A and 4B). Of note, both trajectories express high levels of *KLRC1* although at different degrees of expression, with S0 showing the highest amounts of this gene in the pseudotime tree projection (Figure 4C).

The wide expression of *NKG2A* across all Vδ2 T cell clusters from our scRNA-seq data suggests the presence of extensive transcriptional similarities between NKG2A$^+$ and NKG2A$^-$ Vδ2 T cells. To confirm this, we performed additional experiments

(C) Combined violin dot plots highlighting the expression of selected genes in Vδ2 T cell clusters c0–c5. Selected genes were grouped in the categories of *NKG2A(C)/CD94* gene complex, differentiation status, and cytotoxic markers.
(D) Volcano plot showing DEGs between clusters c5 (*NKG2A^{high}*) and c0–c4 Vδ2 T cell clusters pulled together. Red circles represent genes with statistically significant adjusted p values. Blue and gray circles represent genes adjusted p values that were not statistically significant.

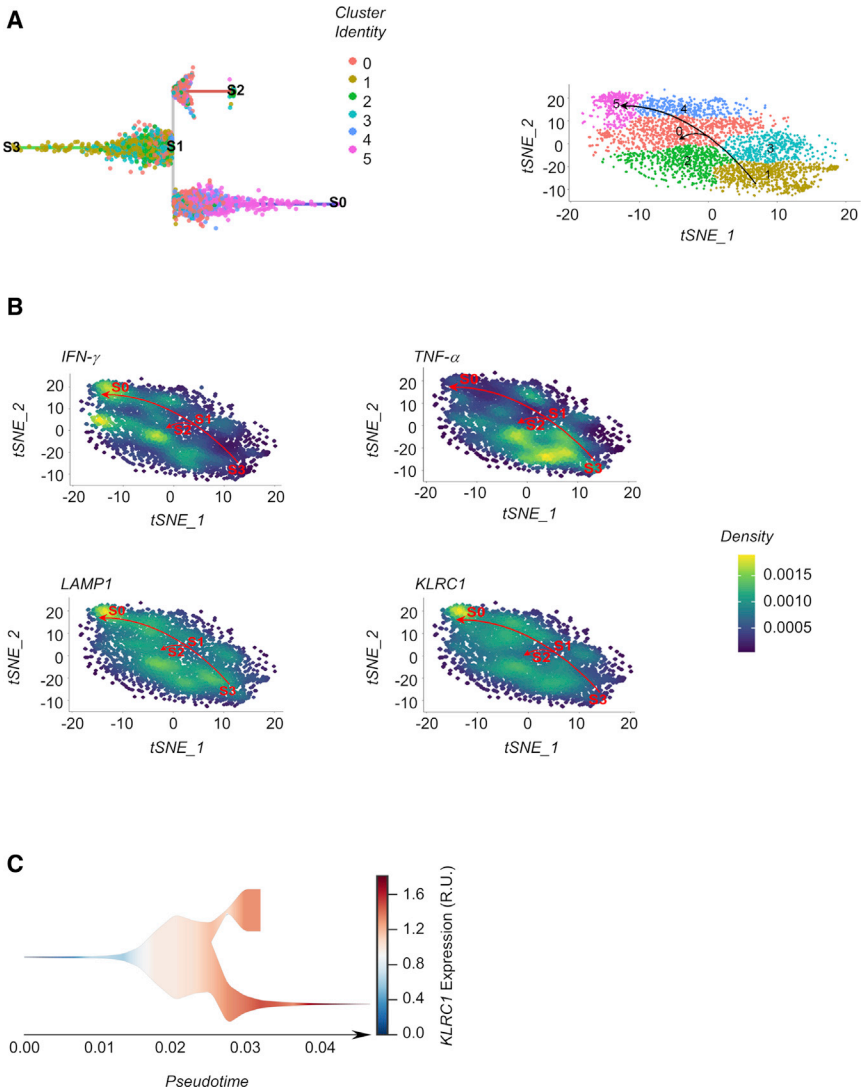

Figure 4. Differentiation and functional transcriptional profile of NKG2A$^+$ and NKG2A$^-$ Vδ2 T cells

(A) Pseudotime plot of total Vδ2 T cells (left) analyzed by scRNA-seq where the different colors of each circle represent cells belonging to the clusters c0–c5. tSNE plot of total Vδ2 T cells (right) with black arrows showing the two main differentiation trajectories identified by the pseudotime analysis.

(B) Expression-weighted two-dimensional kernel density tSNE plots of *INF-γ*, *TNF-α*, *LAMP1* (*CD107a*), and *KLRC1* genes combined with red arrows showing the two main differentiation trajectories of Vδ2 T cells identified by the pseudotime analysis.

(C) Projection of *KLRC1* gene expression on the Vδ2 T cell pseudotime analysis.

of RNA-seq in bulk with fluorescence-activated cell sorting (FACS)-sorted NKG2A$^+$ and NKG2A$^-$ Vδ2 T cells freshly purified from PB of HDs. The transcriptional profiles confirmed the presence of only 26 DEGs (adjusted $p < 0.05$) between the two subsets (Figure S4). Nonetheless, the gene set enrichment analysis (GSEA) clearly indicated that the highest expressions of NKG2A on Vδ2 T cells are associated with the enrichment of signaling pathways involved in the engagement of immune-regulatory and antitumor TNF-α, IFN-γ, IFN-α, and IL-6 cytokines (Figure 5).

Taken together, these findings further confirmed at the transcriptional level that NKG2A$^+$ and NKG2A$^-$ Vδ2 T cells are characterized by two distinct functional programs associated with a differential expression of this checkpoint inhibitor.

NKG2A expression distinguishes two distinct Vδ2 T cell subsets with self-renewal activities

We then investigated the kinetics of phenotypic and functional changes of NKG2A$^+$ and NKG2A$^-$ Vδ2 T cells expanded *in vitro* from PBMCs incubated with zoledronate. Notably, no significant changes were observed in the overall frequencies of NKG2A$^+$ Vδ2 T lymphocytes following cell growth, thus implying that PhAg stimulation does not induce a *de novo* expression of NKG2A. We obtained similar results for the expression of the other members of NKG2-family receptors, NKG2C and NKG2D. In contrast, the proliferation of Vδ2 T cells is associated with a decreased expression of CD28 due to the preferential expansion of T_{EM} cells in both the NKG2A$^+$ and NKG2A$^-$ compartments. Indeed, NKG2A$^+$ and NKG2A$^-$ T_{EM} cell subsets represent the largest fractions of proliferating Vδ2 T cells, as also confirmed by their similar expression of Ki-67 (Figures 6A–6C, S5A, and S5B). Similar to their counterparts freshly purified from PB, *in vitro* expanded NKG2A$^+$ Vδ2 T cells showed significantly higher abilities to degranulate against HLA-E$^-$ K562 compared to NKG2A$^-$ Vδ2 T cells. In addition, the higher performance of NKG2A$^+$ Vδ2 T cells was accompanied by enhanced K562 target cell death (Figure S5C). Again, the CD107a degranulation level of NKG2A$^+$ Vδ2 T cells against HLA-E$^+$ 221.G is very low and does not differ from the one exerted by their NKG2A$^-$ counterparts (Figure 6D). To further confirm the great impact of HLA-E in inhibiting the cytotoxicity of Vδ2 T cells through its binding with NKG2A, we successfully knocked out this lectin-type receptor by using CRISPR/Cas9 technology (Figure 6E). We observed that NKG2A-knocked-out (*NKG2A^{ko}*) Vδ2 T cells show a significant increase in degranulation against HLA-E$^+$ 221.G compared to *NKG2A$^+$* Vδ2 T cells incubated with a control probe (Figures 6F and S5D). The possibility of expanding *in vitro* a subset of hyper-responsive NKG2A$^+$ Vδ2 T cells for protocols of adoptive cell immunotherapies against cancer certainly relies on the stability of this population and its ability to self-renew. To investigate this further, we FACS-sorted NKG2A$^-$ and NKG2A$^+$ Vδ2 T cells

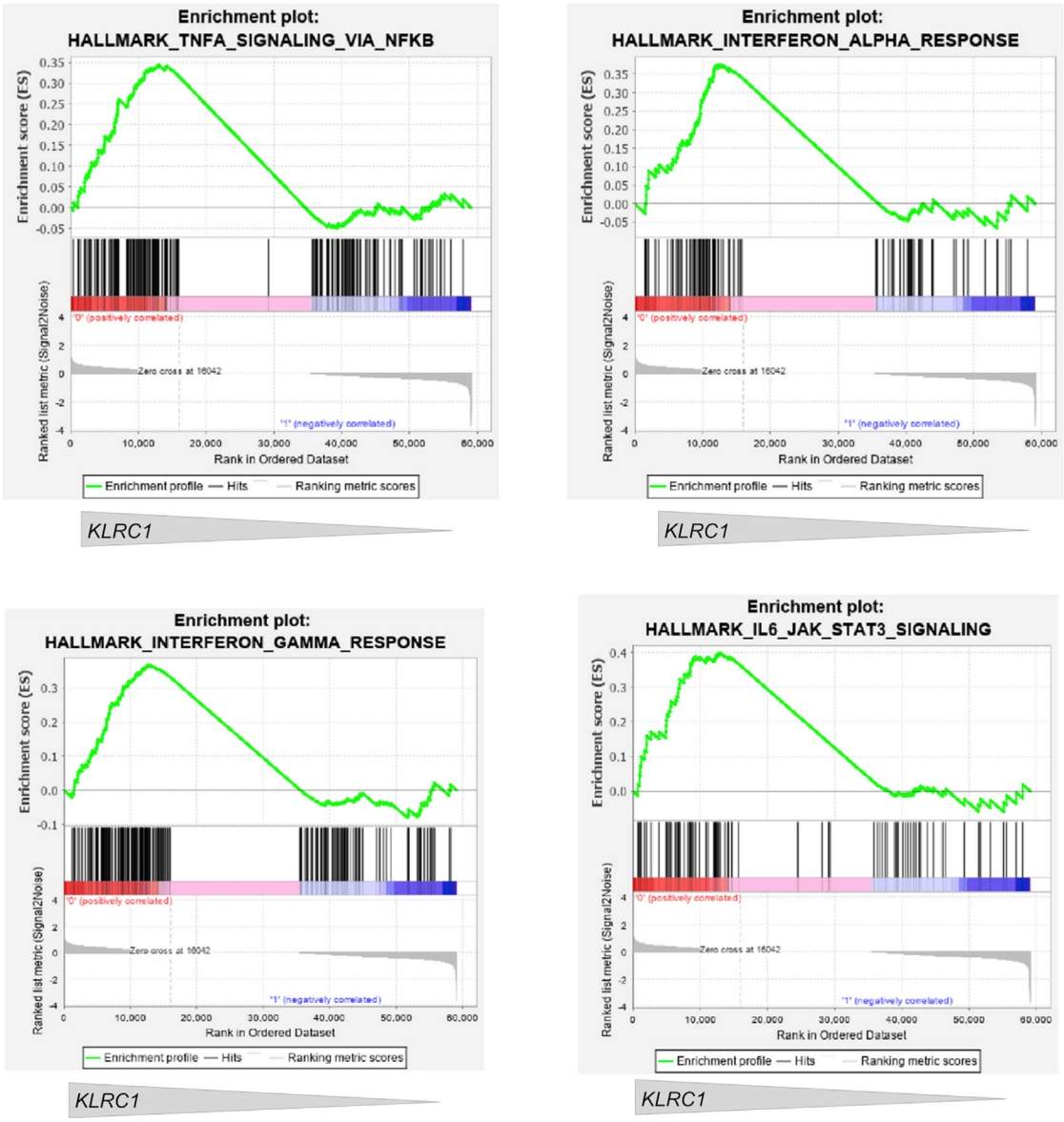

Figure 5. Bulk RNA-seq analysis of the FACS-sorted NKG2A$^+$ and NKG2A$^-$ peripheral blood Vδ2 T cells from healthy donors

Gene set enrichment analyses (GSEAs) performed on sorted NKG2A$^+$ and NKG2A$^-$ Vδ2 T cells and showing the enriched TNF-α, IFN-α, IFN-γ, and IL-6 cytokine signaling pathways in NKG2A$^+$ Vδ2 T cells, respectively. Gray arrows below each graph indicate the gradient of *NKG2A* gene expression.

and put them back in culture in time-course experiments. Our results showed that highly pure and proliferating NKG2A$^+$ and NKG2A$^-$ cells are stable and keep their constitutively high or negative expression of NKG2A after 5 to 6 days of culture, respectively (Figure 6G).

To address the issue of TCR clonality in relation to *KLRC1* expression, we also analyzed the γδTCR repertoire of PB Vδ2 T cells by using scRNA-seq technology (Tan et al., 2020). The results revealed the co-existence of common clones across both *NKG2A*$^+$ and *NKG2A*$^-$ Vδ2 T cells, thus indicating an independent activation and clonal expansion of NKG2A$^+$ and NKG2A$^-$ Vδ2 T cells (Figure 6H).

Finally, we investigated the expression of NKG2A on human postnatal Vδ2 thymocytes. Soon after birth, Vδ2 thymocytes are less frequent compared to Vδ1 thymocytes (Mikulak et al., 2019b). However, 30% of all Vδ2 thymocytes constitutively express NKG2A, which, in contrast, is absent on Vδ1 thymocytes. Notably, *in vitro* expanded Vδ2 thymocytes maintain stable expression of NKG2A, as we did not observe any significant changes in the frequencies of NKG2A$^+$ Vδ2 thymocytes following activation and proliferation *in vitro* (Figures 6I and 6J). This additional set of data demonstrates the existence of two "intralineages" of NKG2A$^+$ and NKG2A$^-$ within the Vδ2 T cell population that appear early during thymic development.

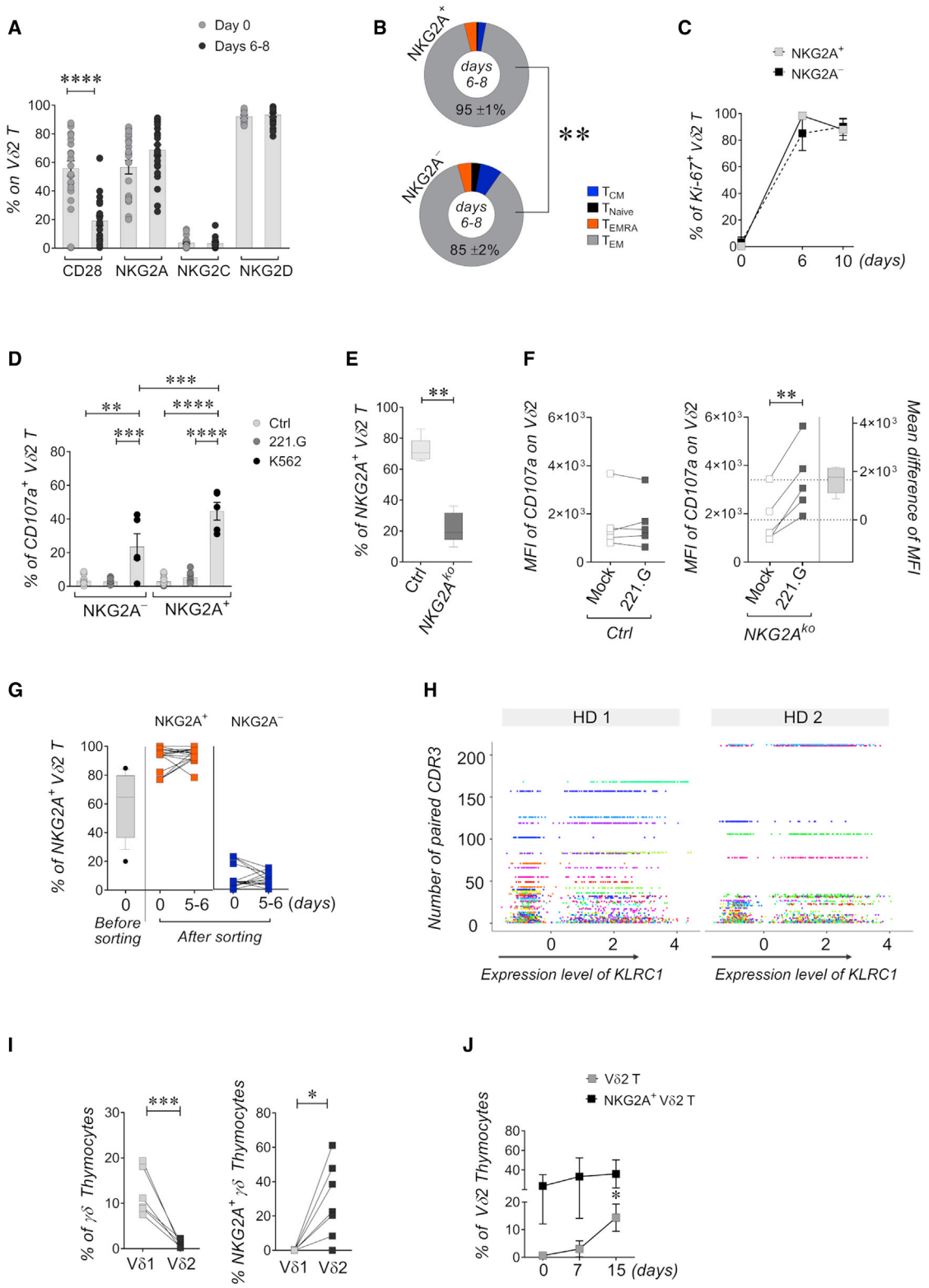

Figure 6. Phenotypic and functional features of NKG2A⁺ Vδ2 T cells expanded *in vitro*

(A) Statistical analysis of flow cytometry data showing the frequency (% ± SEM) of CD28, NKG2A, NKG2C, and NKG2D on Vδ2 T cells expanded *in vitro* (n ≥ 13). (B) Pie charts showing the distribution (% ± SEM) of T_{NAIVE}, T_{CM}, T_{EM}, and T_{EMRA} cell subpopulations in NKG2A⁺ and NKG2A⁻ Vδ2 T cells after 6–8 days of proliferation (n = 23).

(legend continued on next page)

NKG2A$^+$ Vδ2 T cells are recruited into human solid tumors and predict patients' overall survival

In order to understand whether NKG2A$^+$ Vδ2 T cells have a clinical impact on human solid tumors, we used flow cytometry to analyze the phenotype of TILs freshly purified from tumor specimens of patients who had undergone surgical removal of GBM, HCC, and NSCLC. The results first showed that these tumors are characterized by different frequencies of infiltrating Vδ2 and Vδ1 T cells among TILs. However, regardless of the different origin and histology of GBM, HCC, and NSCLC, all of their Vδ2 TILs expressed constitutively high levels of NKG2A. This was not the case for their Vδ1 T counterparts (Figures 7A and 7B). We then compared the expression of NKG2A on Vδ2 T cells in matched PB and tumor samples from the same patients who had undergone surgical procedures. We found that the frequencies of NKG2A$^+$ Vδ2 cells are significantly higher in the tumor mass of GBM and NSCLC compared to PB. As for HCC, although we did not detect any significant difference in the percentages of NKG2A$^+$ Vδ2 T cells between tumor specimens and PB, the overall frequencies of this subset were very high in both anatomic compartments (Figure 7C).

Our preclinical result showed that the antitumor hyper-responsiveness of NKG2A$^+$ Vδ2 T cells is finely tuned by the degree of HLA-E expression on tumor target cell lines. We then proceeded to validate this phenomenon also at the clinical level to possibly predict an effective role for NKG2A$^+$ Vδ2 TILs in modulating progression of aggressive malignancies. To this end, we searched The Cancer Genome Atlas (TCGA; https://www.cancer.gov/about-nci/organization/ccg/research/structural-genomics/tcga) datasets for cohorts of patients affected by GBM, HCC, and NSCLC by using the Gene Expression Profiling Interactive Analysis 2 (GEPIA 2) web server. In line with our flow cytometry analysis, we found a significant correlation between *KLRC1* gene expression and the frequency of Vδ2 T cells in tumor tissues of patients affected by the above-mentioned tumors (Figure 7D). To analyze the impact of NKG2A$^+$ Vδ2 TILs on overall survival (OS), patients were stratified according to the molecular signature of these lymphocytes, referred to as *Vδ2 T-SI*. As previously reported, *Vδ2 T-SI* was defined by the expression of the *CD3E-TRGC1* complex together with the top five upregulated genes (*KLRC1, KLRB1, GZMK, NFKBIA, RORA*) in the transcriptomic profile of Vδ2 T cells compared to their Vδ1 T counterpart (Figure S6A) (Pizzolato et al., 2019). Our results showed that high frequencies of *Vδ2 T-SI* TILs are associated with better patient OS in NSCLC and HCC. These significant correlations were also validated by the comparison of hazard ratios (HRs) and associated 95% confidence intervals (CIs) for different thresholds of the cut-off values (Figures 7E and S6B). Our latter findings are in line with another piece of evidence showing either significantly decreased or stable *HLA-E* expressions in NSCLC or HCC tumor specimens compared to their healthy tissue counterparts (Figure 7E). By contrast, high frequencies of *Vδ2 T-SI* TILs in GBM did not have any impact on patients' OS. This phenomenon couples with the significantly increased expression of *HLA-E* in GBM specimens compared to healthy tissue. Collectively, these findings highlight also at the clinical level the key role played by the degree of HLA-E expression in modulating the hyper-responsiveness of NKG2A$^+$ Vδ2 TILs in different types of solid tumors.

DISCUSSION

The present study identifies a subset of human circulating NKG2A$^+$ Vδ2 T cells that naturally exert the highest antitumor effector functions among the entire Vδ2 T cell population. This experimental evidence resembles the so-called education process first described for NK cells and refers to a phenomenon in which a specific cell subset achieves a constitutive hyperresponsiveness. In particular, the "arming model" theory postulates that the engagement of several inhibitory receptors, including NKG2A, directly potentiates NK cells with a functional surplus (Kim et al., 2005). This theory contradicts current knowledge of inhibitory receptors that negatively regulate downstream signaling upon binding with their putative ligands. However, the alternative employment of inhibitory receptors has been explained with the presence of essential ITIM motifs and recruitment of phosphatases SHP1 and SHP2 (Kim et al., 2005; Viant et al., 2014). We show here that this concept of education can be also extended to those Vδ2 T cells expressing high constitutive levels of NKG2A and supplied with remarkably higher cytokine productions and cytotoxic potential compared to their

(C) Time-course experiments showing the frequencies of the proliferating marker Ki-67 (% ± SEM) on NKG2A$^+$ and NKG2A$^-$ Vδ2 T cells (n = 5).
(D) Statistical analyses of flow cytometry data showing the frequency (% ± SEM) of CD107a on *in vitro* expanded NKG2A$^+$ and NKG2A$^-$ Vδ2 T cells cultured either in the absence (Ctrl in white circles) or presence of HLA-E$^+$ 221.G (gray circles) and HLA-E$^-$ K562 (black circles) tumor cell targets (n ≥ 7).
(E) Statistical analyses of flow cytometry data showing the frequency (% ± SEM) of NKG2A$^+$ Vδ2 T cells expanded *in vitro* and edited with CRISPR/Cas9 to knock out either a nonspecific gene target (Ctrl) or the specific gene-*KLRC1* (*NKG2A^{ko}*) (n = 5).
(F) Statistical analyses of flow cytometry data showing the mean fluorescence intensity (MFI) of CD107a$^+$ Ctrl (left) and *NKG2A^{ko}* (right) Vδ2 T cells incubated either in the absence (mock) or in the presence of HLA-E$^+$ 221.G cells (n = 5).
(G) Time-course experiments showing the frequencies of NKG2A$^+$ Vδ2 T cells (% ± SEM) expanded *in vitro* before and after being FACS-sorted for their surface expression of NKG2A (n = 15).
(H) scRNA-seq (GEO: GSE149356) analysis showing the number of shared CDR3 sequencies (y-axis) in relation to *KLRC1* (*NKG2A*) transcript expression levels (x-axis) in PB Vδ2 T cells isolated from two healthy donors (HD1 and HD2). Cells with an expression level of *NKG2A* higher than 0 were considered *NKG2A*$^+$. Each dot represents a single cell with Vδ2 TCR and each color represents a unique CDR3 sequence.
(I) Statistical analyses of flow cytometry data showing the frequencies (%) of total Vδ1 and Vδ2 thymocytes (left; n = 7) and of NKG2A$^+$ Vδ1 and Vδ2 thymocytes (right; n = 7) freshly purified from the postnatal thymus of healthy donors.
(J) Time-course experiments showing the frequencies (% ± SEM) of total Vδ2 thymocytes (gray squares) and of NKG2A$^+$ Vδ2 thymocytes (black squares) upon *in vitro* expansion (n = 5).
For the comparison of two groups of samples, the paired t test was applied. Experiments with more than two groups were analyzed by ANOVA test with Tukey's comparison test. Statistical differences are represented as p values: *p < 0.05; **p < 0.01; ***p < 0.001; ****p < 0.0001.

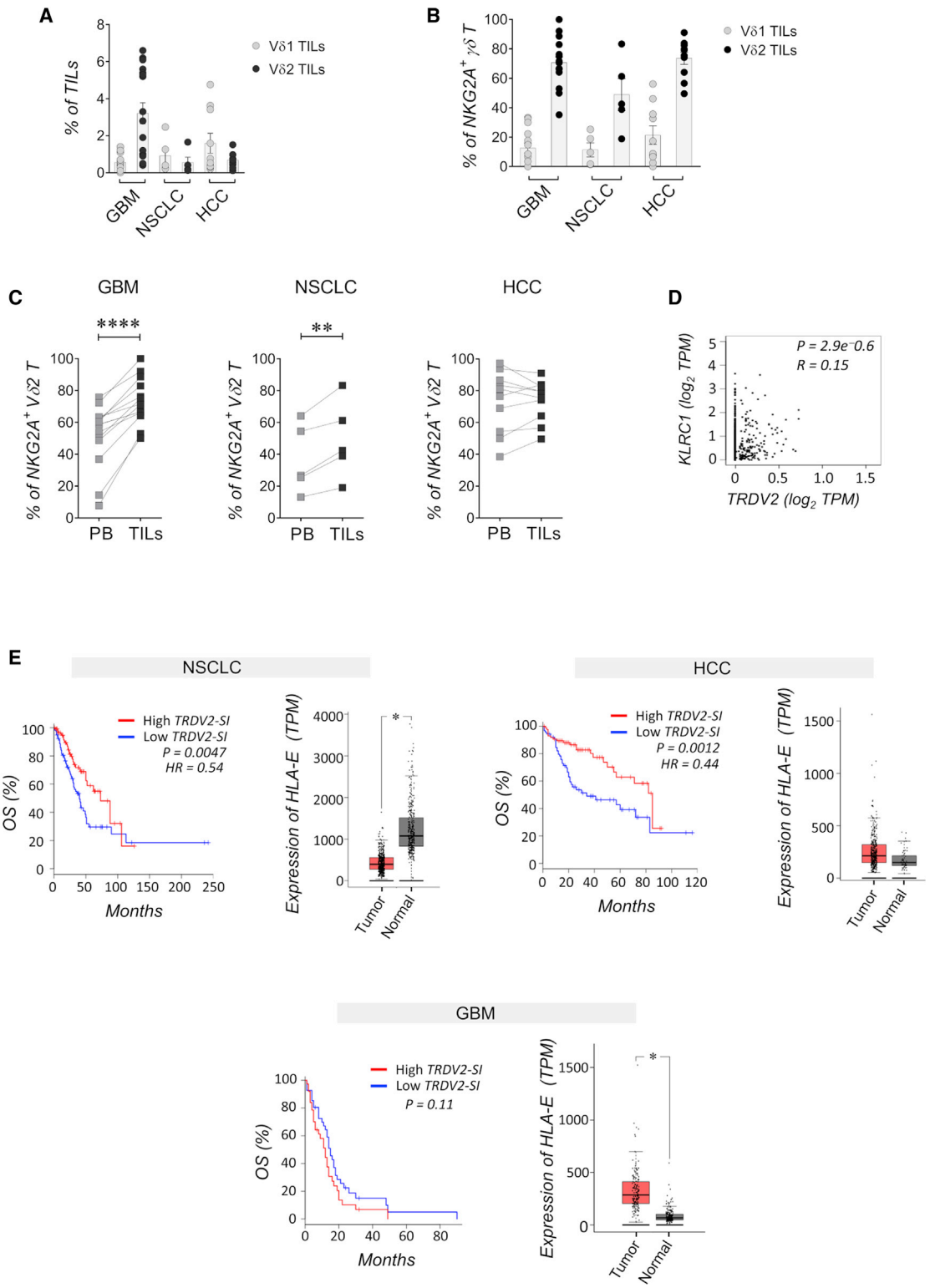

Figure 7. Impact of NKG2A$^+$ Vδ2 tumor-infiltrating lymphocytes in solid human tumors

(A–C) Statistical analysis of flow cytometry data showing the frequencies (% ± SEM) of total Vδ2 and Vδ1 T cells among total tumor-infiltrating lymphocytes (TILs) (A), NKG2A$^+$ Vδ2 and Vδ1 TILs (B), and NKG2A$^+$ Vδ2 TILs in matched samples of tumor and PB (C) from patients affected by glioblastoma (GBM; n = 14), non-small cell lung carcinoma (NSCLC; n = 5), and hepatocellular carcinoma (HCC; n = 10).

(legend continued on next page)

NKG2A$^-$ counterpart. These results are particularly relevant in human health and disease, considering that the existence of a γδ T cell subset reactive to PhAgs has been reported only in alpacas and both human and nonhuman primates but not in mice (Fichtner et al., 2020).

CD94/NKG2A was originally described as a C-lectin-type protein able to prevent cell activation (Moretta et al., 1994). Indeed, our data show that freshly purified circulating NKG2A$^+$ Vδ2 T cells are in a quiescent status under homeostatic conditions as indicated by their low/absent expression of CD69. This observation is consistent with recent findings of Vδ2 T cells being more resilient to the environment compared to Vδ1 T cells (Xu et al., 2019). In contrast, as soon as we trigger the activation/expansion *in vitro* of NKG2A$^+$ Vδ2 T cells with either zoledronate or incubation with tumor cell targets, they acquire a consistent and stable state of hyper-responsiveness. The molecular mechanisms inducing the maximal effector functions are still unknown even for previously reported "educated" NK cells. Cell-to-cell contact constitutes the first step in inducing cell cytotoxicity; in this regard, it has been proposed that "educated" NK cells form stronger contacts with target cells through activating receptors such as NKG2D and NCRs. Instead, activating receptors in "uneducated" NK cells are less confined at the membrane site and are dispersed into the actin meshwork (Guia et al., 2011). We show here that both NKG2A$^+$ and NKG2A$^-$ Vδ2 T cells express high levels of NKG2D, which indeed is one of the key receptors inducing γδ T cell antitumor activities (Correia et al., 2013; Lee et al., 2020). Hence, this mechanism might also apply for "educated" Vδ2 T cells, considering that the expression of human NKG2D ligands (e.g., MHC class I chain-related proteins MICA/B and UL16-binding proteins [ULBP1–ULBP6]) on malignant cells represents a favorable prognostic marker associated with increased patients' OS (Dhar and Wu, 2018; Schmiedel and Mandelboim, 2018; Strid et al., 2008). Nevertheless, our results showed that the direct engagement of γδTCR signaling in the absence of tumor cell targets also induces significantly higher cytokine production from NKG2A$^+$ Vδ2 T cells compared to their NKG2A$^-$ counterpart. These data indicate that hyporesponsive NKG2A$^-$ Vδ2 T cells are intrinsically set with a higher threshold for immunologic reactivity even without the formation of immunological synapses. Hence, the compartmentalization of NKG2D or other activating receptors at synapse sites is unlikely the only mechanism explaining the different functional reactivities between NKG2A$^+$ and NKG2A$^-$ Vδ2 T cells.

"Educated" or mature? There is a question regarding whether the hyper-responsive NKG2A$^+$ Vδ2 T cells are "educated" or at a more mature stage of development. Transcriptional profiling at the single-cell level revealed that the differentiation of Vδ2 T cells is independent from the gained expression of NKG2A that, indeed, is present at high levels since from earlier stages of their maturation. Moreover, both NKG2A$^+$ and NKG2A$^-$ Vδ2 T cell subsets show similar telomere lengths, are stable during *in vitro* manipulation/activation, and maintain the same phenotype while proliferating. scRNA-seq data also showed that NKG2A transcripts are expressed at the highest levels on the Vδ2 T cell cluster supplied with the strongest effector-function potentials, as also confirmed by pseudotime analyses. These results were also confirmed by our additional RNA-seq experiments in bulk, showing that the transcriptional profiles of NKG2A$^+$ and NKG2A$^-$ Vδ2 T cells are similar with only 26 DEGs between the two subsets. Also in this latter experimental setting, GSEA reinforced evidence showing that the enrichment of signaling pathways associated with immune-regulatory and antitumor responses are confined within the Vδ2 T cell compartment expressing the highest amounts of NKG2A transcripts. Taken together, our experimental findings clearly indicate that the expression of NKG2A identifies a subset of Vδ2 T cells "educated" to perform the highest effector functions in response to activation or against tumors. Yet in contrast to what has been reported for NK cells (Zaghi et al., 2019), these results do not definitively rule out a specific role of NKG2A in the ontogenesis of Vδ2 T cells and further investigations are required to address this issue. Indeed, another key question is where and how Vδ2 T cells become NKG2A$^+$. We found that postnatal Vδ2 thymocytes express NKG2A. In this regard, it has been previously shown that Vδ2 T cells isolated from newborn cord blood are CD94$^-$, although the expression of NKG2A was not directly assessed. We show here that postnatal thymocytes express high levels of NKG2A and that its expression is stable in time-course experiments following activation *in vitro*. These data are in line with the recent observation showing that human Vδ2 T cells acquire sensitivity and cytotoxicity early after birth (Papadopoulou et al., 2020; Wragg et al., 2020). Thus, acquisition of NKG2A by Vδ2 T cells is associated with a plastic process in the early stage of life and is also adaptable to environmental changes and pathologic conditions in adulthood.

In addition to disclosing important biologic aspects in regard to the education of Vδ2 T cells, the present study paves the way for important clinical translation of this knowledge. First, we show here that Vδ2 T cells infiltrate solid tumors such as GBM, NSCLC, and HCC at different degrees. Regardless of their frequencies within different human tumors, all Vδ2 TILs express a constitutively high level of NKG2A, thus belonging to the "educated" compartment of Vδ2 T cells. Our data also demonstrate that the degree of infiltration of NKG2A$^+$ Vδ2 T cells can exert a great impact on patients' OS. Interestingly and in line with our preclinical data, the prognostic value of NKG2A$^+$ Vδ2 T depends on the degree of expression of HLA-E on malignant cells in analyzed GBM, NSCLC, and HCC tumors. Indeed, high frequencies of

(D) Spearman correlation between gene expression of *NKG2A* (*KLRC1*) and *TRDV2* (TCR delta variable 2 segment; referred to Vδ2 T cells) measured as the $\log_2$ transcripts per million (TPM) in tumor samples belonging to aggregated TCGA cohorts of patients affected by GBM, NSCLC, and HCC.
(E) GEPIA2 analysis with Kaplan-Meier curves (left) showing the OS (%) in the TCGA cohorts of patients with NSCLC (lung adenocarcinoma; HR, 0.54; 95% CI, 0.7–0.4; n = 240), HCC (HR, 0.44; 95% CI, 0.6–0.3; n = 182), and GBM (n = 81) stratified by the low (blue curve) or high (red curve) *Vδ2 T-SI* expression all obtained with quartile (75%–25%) high cut-off. GEPIA2 comparative analysis showing the *HLA-E* expression (right) in tumor (T) samples matched with TCGA and GETx normal (N) data in patients with GBM (T = 163; N = 207), NSCLC (T = 483; N = 347), and HCC (T = 369; N = 160).
For the comparison of two groups of samples, the paired t test was applied. Experiments with more than two groups were analyzed by ANOVA with Tukey's comparison test. Statistical differences are represented as p values: *p < 0.05; **p < 0.01; ****p < 0.0001.

NKG2A$^+$ Vδ2 TILs significantly improve patients' OS in those tumors like NSCLC and HCC showing decreased/similar levels of HLA-E compared to normal tissue. This is not the case for GBM where the higher expression of HLA-E on malignant cells is coupled with the lack of any clinical impact of NKG2A$^+$ Vδ2 TILs on patients' OS. It is well known that HLA-E is differently expressed on the surfaces of different malignant cells and that inflammation in cancer upregulates the surface levels of HLA-E (Boudreau and Hsu, 2018; Marín et al., 2003). Hence, multivariate analysis matching the degree of HLA-E expression with frequencies of NKG2A$^+$ Vδ2 TILs might serve as a reliable prognostic marker to better predict OS in patients with cancer.

The implementation of adoptive cell transfer therapies administering educated and hyper-responsive NKG2A$^+$ Vδ2 T cells represents another potential clinical application of the knowledge gained by our study. Indeed, there is an urgent unmet need to optimize the efficacy of the current trials administering pools of either γδ or Vδ2 T cells without selecting those effectors endowed with the highest antitumor potential (Godfrey et al., 2018). In this regard, we also have to take into account that targeting NKG2A to unleash the antitumor effector functions of NK and conventional T cells has been proposed for the immunotherapy of solid and hematologic cancers (Andre et al., 2018; Roberto et al., 2018; van Montfoort et al., 2018). Indeed, a humanized anti-NKG2A mAb (IPH2201, monalizumab) has been developed and is currently being tested in several clinical trials (van Hall et al., 2019; Zaghi et al., 2019). Our data suggest that the implementation of customized immunotherapies should take into account the degree of expression of HLA-E on tumor cells (Marín et al., 2003). Indeed, for cancers like GBM expressing high levels of HLA-E, the combined administration of *in vitro* expanded/activated NKG2A$^+$ Vδ2 T cells and anti-NKG2A mAb would greatly enhance antitumor responses by disrupting the inhibition triggered by engagement of the HLA-E-NKG2A checkpoint. However, for tumors like NSCLC and HCC showing low/normal levels of HLA-E and low frequencies of Vδ2 TILs, the infusion alone of educated and hyper-responsive NKG2A$^+$ Vδ2 T cells expanded/activated *in vitro* would provide a more powerful tool to eradicate malignant cells compared to previous adoptive cell transfer trials administering total γδ T cells (Kakimi et al., 2014). Hence, our data indicate that the clinical use of educated NKG2A$^+$ Vδ2 T cells should be matched with the histopathologic features and HLA-E expression of human tumors to tailor those immunotherapy protocols exerting the most powerful immune responses against cancers.

STAR★METHODS

Detailed methods are provided in the online version of this paper and include the following:

SUPPLEMENTAL INFORMATION

Supplemental information can be found online at https://doi.org/10.1016/j.celrep.2021.109871.

ACKNOWLEDGMENTS

We thank the HDs and all patients affected by HCC, NSCLC, and GBM for their generosity and participation in this study, along with all of the nurses and clinicians at the Humanitas Clinical and Research Center IRCCS, in Rozzano, Milan, Italy, and the San Raffaele Scientific Institute in Milan, Italy. We also thank Dr. Ferdinando Oriolo, Dr. Gianmarco Spata, and Dr. Roberta Ciceri for help in processing biological specimens. The NKG2A receptor was first discovered and cloned in 1994 by Prof. Alessandro Moretta and his research team (Moretta et al., 1994). We dedicate this paper to his memory as a great mentor, friend, and visionary scientist.

This work was supported by grants from the Associazione Italiana per la Ricerca sul Cancro (IG 14687 to D.M., 5x1000 21147 to E.M., and IG 20676 to E.L.), the Italian Ministry of Health (Bando Ricerca Finalizzata PE-2016-02363915 to D.M. and RF-2018-12367150 to M.D.), intramural research and clinical funding programs of Humanitas Research Hospital (5x1000 to M.D. and D.M), University of Milan (to D.M.), OR2799 and RESIST (to I.P.), and Compagnia di San Paolo 2019.866 (to E.M.). V.C, C.C and S.F. are recipients of competitive fellowships awarded from the Ph.D program of Experimental Medicine from University of Milan. S.T. is a recipient of competitive fellowship awarded from the Data Science in Medicine and Nutrition (DASMEN) Ph.D program from Humanitas University. The purchase of a FACSSymphony A5 was defrayed in part by a grant from the Italian Ministry of Health (Agreement 82/2015).

AUTHOR CONTRIBUTIONS

V.C., E.B., C.C., S.F., and P.M. performed experiments and analyzed data; S.T. and R.P. performed scRNA-seq analysis; M.D., G.T., M.C., M.S., L.B., A.V., and E.L. recruited patients and obtained human specimens; L.T., S.R., and I.P. performed and analyzed γδTCR-seq analysis; E.M. provided reagents and assistance in the interpretation and analysis of the data; D.S. provided assistance in CRISP-Cas9 gene-editing experiments; E.V. and S.D.B. provided assistance in manuscript preparation; F.S.C. provided reagents and assistance with flow cytometry and cell sorting; and J.M. and D.M. directed and designed the study, analyzed data, and wrote the manuscript.

DECLARATION OF INTERESTS

The authors declare no competing interests.

Received: May 25, 2021
Revised: August 13, 2021
Accepted: September 29, 2021
Published: October 19, 2021

REFERENCES

Abd Hamid, M., Wang, R.Z., Yao, X., Fan, P., Li, X., Chang, X.M., Feng, Y., Jones, S., Maldonado-Perez, D., Waugh, C., et al. (2019). Enriched HLA-E and CD94/NKG2A interaction limits antitumor CD8$^+$ tumor-infiltrating T lymphocyte responses. Cancer Immunol. Res. *7*, 1293–1306.

Aktas, E., Kucuksezer, U.C., Bilgic, S., Erten, G., and Deniz, G. (2009). Relationship between CD107a expression and cytotoxic activity. Cell. Immunol. *254*, 149–154.

Andre, P., Denis, C., Soulas, C., Bourbon-Caillet, C., Lopez, J., Arnoux, T., Blery, M., Bonnafous, C., Gauthier, L., Morel, A., et al. (2018). Anti-NKG2A mAb is a checkpoint inhibitor that promotes anti-tumor immunity by unleashing both T and NK cells. Cell *175*, 1731–1743.e1713.

Angelini, D.F., Zambello, R., Galandrini, R., Diamantini, A., Placido, R., Micucci, F., Poccia, F., Semenzato, G., Borsellino, G., Santoni, A., and Battistini, L. (2011). NKG2A inhibits NKG2C effector functions of γδ T cells: implications in health and disease. J. Leukoc. Biol. *89*, 75–84.

Blank, C.U., Haining, W.N., Held, W., Hogan, P.G., Kallies, A., Lugli, E., Lynn, R.C., Philip, M., Rao, A., Restifo, N.P., et al. (2019). Defining 'T cell exhaustion'. Nat. Rev. Immunol. *19*, 665–674.

Bossard, C., Bézieau, S., Matysiak-Budnik, T., Volteau, C., Laboisse, C.L., Jotereau, F., and Mosnier, J.F. (2012). HLA-E/β2 microglobulin overexpression in colorectal cancer is associated with recruitment of inhibitory immune cells and tumor progression. Int. J. Cancer *131*, 855–863.

Boudreau, J.E., and Hsu, K.C. (2018). Natural killer cell education in human health and disease. Curr. Opin. Immunol. *50*, 102–111.

Bovenschen, N., and Kummer, J.A. (2010). Orphan granzymes find a home. Immunol. Rev. *235*, 117–127.

Brummelman, J., Mazza, E.M.C., Alvisi, G., Colombo, F.S., Grilli, A., Mikulak, J., Mavilio, D., Alloisio, M., Ferrari, F., Lopci, E., et al. (2018). High-dimensional single cell analysis identifies stem-like cytotoxic $CD8^+$ T cells infiltrating human tumors. J. Exp. Med. *215*, 2520–2535.

Bruni, E., Cazzetta, V., Donadon, M., Cimino, M., Torzilli, G., Spata, G., Leonardi, G., Dieli, F., Mikulak, J., and Mavilio, D. (2019). Chemotherapy accelerates immune-senescence and functional impairments of $V\delta2^{pos}$ T cells in elderly patients affected by liver metastatic colorectal cancer. J. Immunother. Cancer *7*, 347.

Caccamo, N., Meraviglia, S., Ferlazzo, V., Angelini, D., Borsellino, G., Poccia, F., Battistini, L., Dieli, F., and Salerno, A. (2005). Differential requirements for antigen or homeostatic cytokines for proliferation and differentiation of human Vgamma9Vdelta2 naive, memory and effector T cell subsets. Eur. J. Immunol. *35*, 1764–1772.

Caccamo, N., Battistini, L., Bonneville, M., Poccia, F., Fournié, J.J., Meraviglia, S., Borsellino, G., Kroczek, R.A., La Mendola, C., Scotet, E., et al. (2006a). CXCR5 identifies a subset of Vgamma9Vdelta2 T cells which secrete IL-4 and IL-10 and help B cells for antibody production. J. Immunol. *177*, 5290–5295.

Caccamo, N., Dieli, F., Wesch, D., Jomaa, H., and Eberl, M. (2006b). Sex-specific phenotypical and functional differences in peripheral human Vgamma9/Vdelta2 T cells. J. Leukoc. Biol. *79*, 663–666.

Caccamo, N., La Mendola, C., Orlando, V., Meraviglia, S., Todaro, M., Stassi, G., Sireci, G., Fournié, J.J., and Dieli, F. (2011). Differentiation, phenotype, and function of interleukin-17-producing human $V\gamma9V\delta2$ T cells. Blood *118*, 129–138.

Chen, H., Albergante, L., Hsu, J.Y., Lareau, C.A., Lo Bosco, G., Guan, J., Zhou, S., Gorban, A.N., Bauer, D.E., Aryee, M.J., et al. (2019). Single-cell trajectories reconstruction, exploration and mapping of omics data with STREAM. Nat. Commun. *10*, 1903.

Correia, D.V., Lopes, A., and Silva-Santos, B. (2013). Tumor cell recognition by γδ T lymphocytes: T-cell receptor vs. NK-cell receptors. OncoImmunology *2*, e22892.

Davey, M.S., Willcox, C.R., Hunter, S., Kasatskaya, S.A., Remmerswaal, E.B.M., Salim, M., Mohammed, F., Bemelman, F.J., Chudakov, D.M., Oo, Y.H., and Willcox, B.E. (2018). The human $V\delta2^+$ T-cell compartment comprises distinct innate-like $V\gamma9^+$ and adaptive $V\gamma9^-$ subsets. Nat. Commun. *9*, 1760.

Dhar, P., and Wu, J.D. (2018). NKG2D and its ligands in cancer. Curr. Opin. Immunol. *51*, 55–61.

Eberl, M., Hintz, M., Reichenberg, A., Kollas, A.K., Wiesner, J., and Jomaa, H. (2003). Microbial isoprenoid biosynthesis and human gammadelta T cell activation. FEBS Lett. *544*, 4–10.

Fichtner, A.S., Karunakaran, M.M., Gu, S., Boughter, C.T., Borowska, M.T., Starick, L., Nöhren, A., Göbel, T.W., Adams, E.J., and Herrmann, T. (2020). Alpaca (*Vicugna pacos*), the first nonprimate species with a phosphoantigen-reactive $V\gamma9V\delta2$ T cell subset. Proc. Natl. Acad. Sci. USA *117*, 6697–6707.

Gober, H.J., Kistowska, M., Angman, L., Jenö, P., Mori, L., and De Libero, G. (2003). Human T cell receptor gammadelta cells recognize endogenous mevalonate metabolites in tumor cells. J. Exp. Med. *197*, 163–168.

Godfrey, D.I., Le Nours, J., Andrews, D.M., Uldrich, A.P., and Rossjohn, J. (2018). Unconventional T cell targets for cancer immunotherapy. Immunity *48*, 453–473.

Gooden, M., Lampen, M., Jordanova, E.S., Leffers, N., Trimbos, J.B., van der Burg, S.H., Nijman, H., and van Hall, T. (2011). HLA-E expression by gynecological cancers restrains tumor-infiltrating $CD8^+$ T lymphocytes. Proc. Natl. Acad. Sci. USA *108*, 10656–10661.

Guia, S., Jaeger, B.N., Piatek, S., Mailfert, S., Trombik, T., Fenis, A., Chevrier, N., Walzer, T., Kerdiles, Y.M., Marguet, D., et al. (2011). Confinement of activating receptors at the plasma membrane controls natural killer cell tolerance. Sci. Signal. *4*, ra21.

He, Y., and Tian, Z. (2017). NK cell education via nonclassical MHC and non-MHC ligands. Cell. Mol. Immunol. *14*, 321–330.

Held, W. (2012). Nonclassical NK cell education. Nat. Immunol. *13*, 1135–1137.

Hudspeth, K., Fogli, M., Correia, D.V., Mikulak, J., Roberto, A., Della Bella, S., Silva-Santos, B., and Mavilio, D. (2012). Engagement of NKp30 on Vδ1 T cells induces the production of CCL3, CCL4, and CCL5 and suppresses HIV-1 replication. Blood *119*, 4013–4016.

Hudspeth, K., Silva-Santos, B., and Mavilio, D. (2013). Natural cytotoxicity receptors: broader expression patterns and functions in innate and adaptive immune cells. Front. Immunol. *4*, 69.

Ismaili, J., Olislagers, V., Poupot, R., Fournié, J.J., and Goldman, M. (2002). Human gamma delta T cells induce dendritic cell maturation. Clin. Immunol. *103*, 296–302.

Ivarsson, M.A., Loh, L., Marquardt, N., Kekäläinen, E., Berglin, L., Björkström, N.K., Westgren, M., Nixon, D.F., and Michaëlsson, J. (2013). Differentiation and functional regulation of human fetal NK cells. J. Clin. Invest. *123*, 3889–3901.

Joncker, N.T., Fernandez, N.C., Treiner, E., Vivier, E., and Raulet, D.H. (2009). NK cell responsiveness is tuned commensurate with the number of inhibitory receptors for self-MHC class I: the rheostat model. J. Immunol. *182*, 4572–4580.

Kabat, J., Borrego, F., Brooks, A., and Coligan, J.E. (2002). Role that each NKG2A immunoreceptor tyrosine-based inhibitory motif plays in mediating the human CD94/NKG2A inhibitory signal. J. Immunol. *169*, 1948–1958.

Kaiser, B.K., Pizarro, J.C., Kerns, J., and Strong, R.K. (2008). Structural basis for NKG2A/CD94 recognition of HLA-E. Proc. Natl. Acad. Sci. USA *105*, 6696–6701.

Kakimi, K., Matsushita, H., Murakawa, T., and Nakajima, J. (2014). γδ T cell therapy for the treatment of non-small cell lung cancer. Transl. Lung Cancer Res. *3*, 23–33.

Kim, S., Poursine-Laurent, J., Truscott, S.M., Lybarger, L., Song, Y.J., Yang, L., French, A.R., Sunwoo, J.B., Lemieux, S., Hansen, T.H., and Yokoyama, W.M. (2005). Licensing of natural killer cells by host major histocompatibility complex class I molecules. Nature *436*, 709–713.

Kishi, A., Takamori, Y., Ogawa, K., Takano, S., Tomita, S., Tanigawa, M., Niman, M., Kishida, T., and Fujita, S. (2002). Differential expression of granulysin and perforin by NK cells in cancer patients and correlation of impaired granulysin expression with progression of cancer. Cancer Immunol. Immunother. *50*, 604–614.

Kondo, M., Izumi, T., Fujieda, N., Kondo, A., Morishita, T., Matsushita, H., and Kakimi, K. (2011). Expansion of human peripheral blood γδ T cells using zoledronate. J. Vis. Exp. (*55*), 3182.

Kurioka, A., Cosgrove, C., Simoni, Y., van Wilgenburg, B., Geremia, A., Björkander, S., Sverremark-Ekström, E., Thurnheer, C., Günthard, H.F., Khanna, N., et al.; Swiss HIV Cohort Study; Oxford IBD Cohort Investigators (2018). CD161 defines a functionally distinct subset of pro-inflammatory natural killer cells. Front. Immunol. *9*, 486.

Lee, H.W., Chung, Y.S., and Kim, T.J. (2020). Heterogeneity of human γδ T cells and their role in cancer immunity. Immune Netw. *20*, e5.

Long, E.O., Kim, H.S., Liu, D., Peterson, M.E., and Rajagopalan, S. (2013). Controlling natural killer cell responses: integration of signals for activation and inhibition. Annu. Rev. Immunol. *31*, 227–258.

Lorenzo-Herrero, S., Sordo-Bahamonde, C., Gonzalez, S., and López-Soto, A. (2019). CD107a degranulation assay to evaluate immune cell antitumor activity. Methods Mol. Biol. *1884*, 119–130.

Marín, R., Ruiz-Cabello, F., Pedrinaci, S., Méndez, R., Jiménez, P., Geraghty, D.E., and Garrido, F. (2003). Analysis of HLA-E expression in human tumors. Immunogenetics *54*, 767–775.

Mikulak, J., Dieli, F., and Mavilio, D. (2019a). Are human Vδ2^{pos} T cells really resistant to aging and human cytomegalovirus infection? EBioMedicine *43*, 30.

Mikulak, J., Oriolo, F., Bruni, E., Roberto, A., Colombo, F.S., Villa, A., Bosticardo, M., Bortolomai, I., Lo Presti, E., Meraviglia, S., et al. (2019b). NKp46-expressing human gut-resident intraepithelial Vδ1 T cell subpopulation exhibits high antitumor activity against colorectal cancer. JCI Insight *4*, e125884.

Mingari, M.C., Ponte, M., Bertone, S., Schiavetti, F., Vitale, C., Bellomo, R., Moretta, A., and Moretta, L. (1998). HLA class I-specific inhibitory receptors in human T lymphocytes: interleukin 15-induced expression of CD94/NKG2A in superantigen- or alloantigen-activated CD8+ T cells. Proc. Natl. Acad. Sci. USA *95*, 1172–1177.

Mingari, M.C., Pietra, G., and Moretta, L. (2019). Immune checkpoint inhibitors: anti-NKG2A antibodies on board. Trends Immunol. *40*, 83–85.

Moretta, A., Vitale, M., Sivori, S., Bottino, C., Morelli, L., Augugliaro, R., Barbaresi, M., Pende, D., Ciccone, E., Lopez-Botet, M., and Moretta, L. (1994). Human natural killer cell receptors for HLA-class I molecules. Evidence that the Kp43 (CD94) molecule functions as receptor for HLA-B alleles. J. Exp. Med. *180*, 545–555.

Papadopoulou, M., Dimova, T., Shey, M., Briel, L., Veldtsman, H., Khomba, N., Africa, H., Steyn, M., Hanekom, W.A., Scriba, T.J., et al. (2020). Fetal public Vγ9Vδ2 T cells expand and gain potent cytotoxic functions early after birth. Proc. Natl. Acad. Sci. USA *117*, 18638–18648.

Pizzolato, G., Kaminski, H., Tosolini, M., Franchini, D.M., Pont, F., Martins, F., Valle, C., Labourdette, D., Cadot, S., Quillet-Mary, A., et al. (2019). Single-cell RNA sequencing unveils the shared and the distinct cytotoxic hallmarks of human TCRVδ1 and TCRVδ2 γδ T lymphocytes. Proc. Natl. Acad. Sci. USA *116*, 11906–11915.

Ribot, J.C., Lopes, N., and Silva-Santos, B. (2021). γδ T cells in tissue physiology and surveillance. Nat. Rev. Immunol. *21*, 221–232.

Roberto, A., Di Vito, C., Zaghi, E., Mazza, E.M.C., Capucetti, A., Calvi, M., Tentorio, P., Zanon, V., Sarina, B., Mariotti, J., et al. (2018). The early expansion of anergic NKG2A^{pos}/CD56^{dim}/CD16^{neg} natural killer represents a therapeutic target in haploidentical hematopoietic stem cell transplantation. Haematologica *103*, 1390–1402.

Schmiedel, D., and Mandelboim, O. (2018). NKG2D ligands-critical targets for cancer immune escape and therapy. Front. Immunol. *9*, 2040.

Sebestyen, Z., Prinz, I., Déchanet-Merville, J., Silva-Santos, B., and Kuball, J. (2020). Translating gammadelta (γδ) T cells and their receptors into cancer cell therapies. Nat. Rev. Drug Discov. *19*, 169–184.

Strid, J., Roberts, S.J., Filler, R.B., Lewis, J.M., Kwong, B.Y., Schpero, W., Kaplan, D.H., Hayday, A.C., and Girardi, M. (2008). Acute upregulation of an NKG2D ligand promotes rapid reorganization of a local immune compartment with pleiotropic effects on carcinogenesis. Nat. Immunol. *9*, 146–154.

Stuart, T., Butler, A., Hoffman, P., Hafemeister, C., Papalexi, E., Mauck, W.M., 3rd, Hao, Y., Stoeckius, M., Smibert, P., and Satija, R. (2019). Comprehensive integration of single-cell data. Cell *177*, 1888–1902.e1821.

Tan, L., Fichtner, A.S., Bubke, A., Odak, I., Schultze-Florey, C., Koenecke, C., Förster, R., Jarek, M., Von Kaisenberg, C., Borchers, A., et al. (2020). A fetal wave of human type-3 γδ T cells with restricted TCR diversity persists into adulthood. bioRxiv. https://doi.org/10.1101/2020.08.14.248146.

Taveirne, S., Filtjens, J., Van Ammel, E., De Colvenaer, V., Kerre, T., Taghon, T., Vandekerckhove, B., Plum, J., Held, W., and Leclercq, G. (2011). Inhibitory receptors specific for MHC class I educate murine NK cells but not CD8αα intestinal intraepithelial T lymphocytes. Blood *118*, 339–347.

Tierney, J.F., Stewart, L.A., Ghersi, D., Burdett, S., and Sydes, M.R. (2007). Practical methods for incorporating summary time-to-event data into meta-analysis. Trials *8*, 16.

van Hall, T., André, P., Horowitz, A., Ruan, D.F., Borst, L., Zerbib, R., Narni-Mancinelli, E., van der Burg, S.H., and Vivier, E. (2019). Monalizumab: inhibiting the novel immune checkpoint NKG2A. J. Immunother. Cancer *7*, 263.

van Montfoort, N., Borst, L., Korrer, M.J., Sluijter, M., Marijt, K.A., Santegoets, S.J., van Ham, V.J., Ehsan, I., Charoentong, P., Andre, P., et al. (2018). NKG2A blockade potentiates CD8 T cell immunity induced by cancer vaccines. Cell *175*, 1744–1755.e1715.

Vantourout, P., and Hayday, A. (2013). Six-of-the-best: unique contributions of γδ T cells to immunology. Nat. Rev. Immunol. *13*, 88–100.

Viant, C., Fenis, A., Chicanne, G., Payrastre, B., Ugolini, S., and Vivier, E. (2014). SHP-1-mediated inhibitory signals promote responsiveness and anti-tumour functions of natural killer cells. Nat. Commun. *5*, 5108.

Wang, L., Das, H., Kamath, A., and Bukowski, J.F. (2001). Human V gamma 2V delta 2 T cells produce IFN-gamma and TNF-alpha with an on/off/on cycling pattern in response to live bacterial products. J. Immunol. *167*, 6195–6201.

Wragg, K.M., Tan, H.X., Kristensen, A.B., Nguyen-Robertson, C.V., Kelleher, A.D., Parsons, M.S., Wheatley, A.K., Berzins, S.P., Pellicci, D.G., Kent, S.J., and Juno, J.A. (2020). High CD26 and low CD94 expression identifies an IL-23 responsive Vδ2^{+} T cell subset with a MAIT cell-like transcriptional profile. Cell Rep. *31*, 107773.

Wu, Z., Liang, J., Wang, Z., Li, A., Fan, X., and Jiang, T. (2020). HLA-E expression in diffuse glioma: relationship with clinicopathological features and patient survival. BMC Neurol. *20*, 59.

Xu, W., Monaco, G., Wong, E.H., Tan, W.L.W., Kared, H., Simoni, Y., Tan, S.W., How, W.Z.Y., Tan, C.T.Y., Lee, B.T.K., et al. (2019). Mapping of γ/δ T cells reveals Vδ2+ T cells resistance to senescence. EBioMedicine *39*, 44–58.

Yawata, M., Yawata, N., Draghi, M., Partheniou, F., Little, A.M., and Parham, P. (2008). MHC class I-specific inhibitory receptors and their ligands structure diverse human NK-cell repertoires toward a balance of missing self-response. Blood *112*, 2369–2380.

Zaghi, E., Calvi, M., Marcenaro, E., Mavilio, D., and Di Vito, C. (2019). Targeting NKG2A to elucidate natural killer cell ontogenesis and to develop novel immune-therapeutic strategies in cancer therapy. J. Leukoc. Biol. *105*, 1243–1251.

Zou, C., Zhao, P., Xiao, Z., Han, X., Fu, F., and Fu, L. (2017). γδ T cells in cancer immunotherapy. Oncotarget *8*, 8900–8909.

STAR★METHODS

KEY RESOURCES TABLE

REAGENT or RESOURCE	SOURCE	IDENTIFIER
Antibodies		
BUV661 Mouse Anti-Human CD3 (clone: UCHT1)	BD Biosciences	Cat# 565065; RRID: AB_2744389
BUV805 Mouse Anti-Human CD8 (clone: SK1)	BD Biosciences	Cat# 564912; RRID: AB_2744465
BUV496 Mouse Anti-Human CD16 (clone: 3G8)	BD Biosciences	Cat# 564653; RRID: AB_2744294
Alexa Fluor® 700 Mouse Anti-Human CD45 (clone: HI30)	BD Biosciences	Cat# 560566; RRID: AB_1645452
BUV737 Mouse Anti-Human CD45RA (clone: HI100)	BD Biosciences	Cat# 612846; RRID: AB_2870168
BUV563 Mouse Anti-Human CD56 (clone: NCAM16.2)	BD Biosciences	Cat# 565704; RRID: AB_2744431
BV650 Mouse Anti-Human CD86 (clone: 2331)	BD Biosciences	Cat# 563411; RRID: AB_2744456
PE Mouse Anti-Human CD107a (clone: H4A3)	BD Biosciences	Cat# 555801; RRID: AB_396135
PE-Cy5 Mouse Anti-Human CD107a (clone: H4A3)	BD Biosciences	Cat# 555802; RRID: AB_396136
BV711 Mouse Anti-Human NKG2A (CD159a) (clone: 131411)	BD Biosciences	Cat# 747919; RRID: AB_2872380
BV786 Mouse Anti-Human CD314 (NKG2D) (clone: 1D11)	BD Biosciences	Cat# 743560; RRID: AB_2741584
BV711 Mouse Anti-Human CD279 (PD-1) (clone: EH12.1)	BD Biosciences	Cat# 564017; RRID: AB_2738543
BUV395 Mouse Anti-Human Vδ2 TCR (clone: B6)	BD Biosciences	Cat# 743754; RRID: AB_2741722
FITC Mouse Anti-Human Ki-67 (clone: B56)	BD Biosciences	Cat# 51-36524X; RRID: AB_396302
TCR Vδ2-FITC Conjugated Antibody (clone: IMMU 389)	Beckman Coulter	Cat# IM1464; RRID: AB_131019
Brilliant Violet 650 anti-human CD3 Antibody (clone: OKT3)	BioLegend	Cat# 317324; RRID: AB_2563352
PE/Cyanine7 anti-human CD3 Antibody (clone: UCHT1)	BioLegend	Cat# 300420; RRID: AB_439781
PE/Cyanine7 anti-human CD28 Antibody (clone: CD28.2)	BioLegend	Cat# 302926; RRID: AB_10644005
Brilliant Violet 605 anti-human CD69 Antibody (clone: FN50)	BioLegend	Cat# 310938; RRID: AB_2562307
Brilliant Violet 421 anti-human CD161 Antibody (clone: HP-3G10)	BioLegend	Cat# 339913; RRID: AB_10915270
PE/Cyanine7 anti-human IFN-gamma Antibody (clone: B27)	BioLegend	Cat# 506518; RRID: AB_2123321
Brilliant Violet 785 anti-human TNF-alpha (clone: MAb11)	BioLegend	Cat# 502948; RRID: AB_2565858
Brilliant Violet 570 anti-human IL-17A Antibody (clone: BL168)	BioLegend	Cat# 512324; RRID: AB_2563886
PE/Cyanine7 anti-human HLA-E Antibody (clone: 3D12)	BioLegend	Cat# 342608; RRID: AB_2565263
VioBright-FITC anti-human NKG2A (CD159a) Antibody (clone: REA110)	Miltenyi Biotec	Cat# 130-105-646; RRID: AB_2655382
APC anti-human NKG2A (CD159a) Antibody (clone: REA110)	Miltenyi Biotec	Cat# 130-098-812; RRID: AB_2655386
APC anti-human NKG2C (CD159c) Antibody (clone: REA205)	Miltenyi Biotec	Cat# 130-103-636; RRID: AB_2655396
PE-Vio615 anti-human CD57 Antibody (clone: REA769)	Miltenyi Biotec	Cat# 130-111-815; RRID: AB_2658752
PE anti-human TCR-Vδ1 Antibody (clone: REA173)	Miltenyi Biotec	Cat# 130-100-535; RRID: AB_2653954
PE-Vio770 anti-human TCR-Vδ1 Antibody (clone: REA173)	Miltenyi Biotec	Cat# 130-100-540; RRID: AB_2653962
CD27 Antibody, APC-eFluor® 780 (clone: O323)	Thermo Fisher Scientific	Cat# 47-0279-42; RRID: AB_1272040
Anti-CD94 blocking mAb Y9	Prof. E. Marcenaro, University of Genoa	N/A
Biological samples		
Healthy human whole blood	Humanitas Research Hospital	N/A
Whole blood and liver tissue from HCC patients	Humanitas Research Hospital	N/A
Whole blood and GBM tissue from GBM patients	Humanitas Research Hospital	N/A
Whole blood and lung tissue from NSCLC patients	Humanitas Research Hospital	N/A
Human healthy thymus	TIGET/San Raffaele Institute	N/A
Chemicals, peptides, and recombinant proteins		
Lympholyte®-H Cell Separation Media	Cedarlane Laboratories	Cat# CL5020
Collagenase D from Clostridium histolyticum	Sigma Aldrich	Cat# 11088882001

(*Continued on next page*)

Continued

REAGENT or RESOURCE	SOURCE	IDENTIFIER
Percoll density gradient media	Cytiva	Cat# 17089101
Zombie Aqua fixable viability kit	BioLegend	Cat# 423102
Paraformaldehyde solution 4% in PBS	Santa Cruz Biotechnology	Cat# sc-281692
Recombinant human IL-15	Peprotech	Cat# 200-15
Zoledronic acid monohydrate	Sigma Aldrich	Cat# SML0223
Recombinant human IL-2	Peprotech	Cat# 200-02
GolgiPlug Protein Transport Inhibitor	BD Biosciences	Cat# 555029
Cytofix/Cytoperm Fixation/Permeabilization kit	BD Biosciences	Cat# 554714
BS3 (bis(sulfosuccinimidyl)suberate), No-Weigh Format	Thermo Fisher Scientific	Cat# A39266
Alt-R® Cas9 Electroporation Enhancer	IDT	Cat# 1075916
Foxp3 / Transcription Factor Staining Buffer Set	Thermo Fisher Scientific	Cat# 00-5523-00
Critical commercial assays		
Telomere PNA Kit/FITC for Flow Cytometry	Dako	Cat# K5327
FITC Annexin V Apoptosis Detection Kit with PI	Immunostep	Cat# ANXVKF-100T
Human T Cell Nucleofector™ Kit	Lonza	Cat# VPA-1002
CMV IgG ELISA Kit	Dia.Pro	Cat# CMVG.CE
Deposited data		
Raw matrix counts	Pizzolato et al. (2019)	GEO: GSE128223 https://www.ncbi.nlm.nih.gov/geo/query/acc.cgi?acc=GSE128223
Paired scRNA-seq and scTCR-seq dataset	Tan et al. (2020)	GEO: GSE149356
TCGA	GEPIA2; http://gepia2.cancer-pku.cn/#index	https://www.cancer.gov/about-nci/organization/ccg/research/structural-genomics/tcga
Experimental models: Cell lines		
K562 cells	ATCC	CCL-243
721.221.G cells	Prof. E. Marcenaro, University of Genoa	N/A
1301 cells	Sigma Aldrich	Cat# 85112105
Oligonucleotides		
Alt-R® CRISPR-Cas9 crRNAs anti-human *KLRC1*	IDT	ID gRNA: Hs.Cas9.KLRC1.1.AA
Alt-R® CRISPR-Cas9 crRNAs negative control	IDT	Cat# 1072544
Alt-R® CRIPSR-Cas9 tracrRNA ATTOTM 550	IDT	Cat# 1075928
Alt-R® S.p. HiFi Cas9 Nuclease V3	IDT	Cat# 1081061
Primer GPO-1 (5′-ACTCCTACGGGAGGCAGCAGT-3′)	Mikulak et al. (2019b)	N/A
Primer MGSO (5′-TGCACCATCTGTCACTCTGTTAACCTC-3′)	Mikulak et al. (2019b)	N/A
Software and algorithms		
FlowJo v9.9.6	TreeStar	https://www.flowjo.com/
Prism 7	GraphPad	https://www.graphpad.com/scientific-software/prism/
Seurat package v3.1.1	Stuart et al., 2019	https://cloud.r-projectorg/package=Seurat
R v3.6.1	R-project	https://www.r-project.org/
Stream	Chen et al. (2019)	https://stream.pinellolab.partners.org/
Other		
gentleMACS Dissociator	Miltenyi Biotec	Cat# 130-093-235
Falcon® 100 μm Cell Strainer	Corning	Cat# 352360
Hank's Balanced salt solution buffer without Ca^{2+} and Mg^{2+}	Euroclone SpA	Cat# ECM0507L

(*Continued on next page*)

Continued

REAGENT or RESOURCE	SOURCE	IDENTIFIER
Fetal Bovine Serum	Sigma Aldrich	Cat# F6524
DMSO	Sigma Aldrich	Cat# 67-68-5
Falcon® 70 μm Cell Strainer	Corning	Cat# 352350
Physiological saline solution (0,9%)	Baxter	Cat# A030942623
Iscove's Modified Dulbecco's medium	Euroclone SpA	Cat# ECB2072L
Penicillin-Streptomycin	Lonza	Cat# DE17-602E
Roswell Park Memorial Institute's medium	Euroclone SpA	Cat# ECB9006L
Pen/Strep/Amphotericin B	Lonza	Cat# 17-745E
Ultraglutamine	Lonza	Cat# BE17-605 E/U1
Falcon® 96-well Clear Round Bottom TC-treated Cell Culture Microplate	Corning	Cat# 353077
BD FACSymphony A5	BD Biosciences	N/A
BD FACS Melody cell sorter	BD Biosciences	N/A
X-VIVO 15 serum-free hematopoietic cell medium	Lonza	Cat# BE02-060F
Human serum	Euroclone SpA	Cat# ECS0219D
Sodium Pyruvate Solution (100 mM)	Lonza	Cat# BE13-115E
NEAA Mixture (100X)	Lonza	Cat# BE13-114E

RESOURCE AVAILABILITY

Lead contact

Further information and requests for resources and reagents should be directed to and will be fulfilled by the lead contact, Domenico Mavilio (domenico.mavilio@unimi.it).

Materials availability

This study did not generate new unique reagents.

Data and code availability

- This paper analyzes existing, publicly available data. Accession numbers for the datasets are listed in the key resources table.
- This paper does not report original code.
- Any additional information required to reanalyze the data reported in this paper is available from the lead contact upon request.

EXPERIMENTAL MODEL AND SUBJECT DETAILS

Patients' recruitment

Recruitment of patients and healthy volunteers have been performed according to the Declaration of Helsinki and all individuals signed written informed consent. PB of 76 HDs were obtained from buffy coats in accordance with clinical and research protocols approved by the Institutional Review Board (IRB) of Humanitas Research Hospital (HRH) (approval 28/01/2016). HDs included both men (73%) and women (27%) with a mean age of 47 years old. Plasma of 24 HDs was analyzed for the presence of HCMV IgG antibodies according to the manufacturer's instructions (Dia.Pro). Patients underwent to liver surgery for HCC *(n = 10; mean age = 77 years; 8 males; 2 females*) were recruited at the Hepatobiliary and General Surgery Department of HRH, for GBM (n = *14; mean age = 58 years; 8 males; 6 females*) at the Unit of Oncological Neurosurgery of HRH, for NSCLC (n = *5; mean age = 64 years; 3 males; 2 females*) at Division of Thoracic Surgery of HRH in accordance with clinical protocols approved by the IRB (approvals 168/18, 118/17, 1501, and 1021). We also received the IRB of TIGET/San Raffaele Institute for specimens of healthy thymus from 7 pediatric patients (*mean age = 15.5 months; 3 males, 4 females*) undergoing cardiac surgery (approval TIGET07, TCTO-044). Parents with the custody of the child undergoing cardiac surgery were informed about the aims of this research program and signed a detailed informed consent.

Human specimens and cell culture

Peripheral blood mononuclear cells (PBMCs) were isolated from buffy coats of HDs or from freshly isolated blood of patients affected by HCC, GBM and NSCLC through *Lympholyte*® Cell Separation density gradient solution (Cederlane Laboratories; Burlington, Canada) according to the manufacturer's instruction.

Freshly isolated HCC liver tissue was dissociated by enzymatic digestion in gentleMACS Dissociator (Miltenyi; Bergisch Gladbach, Germany) with 2 mg/mL of collagenase D (Sigma Aldrich; St. Louis, Missouri, USA) for 45 minutes at 37°C/5% CO_2. Cells were then filtered through 100 μm cell strainer (Corning; New York, USA) and washed in Hank's Balanced salt solution buffer without Ca^{2+} and Mg^{2+} (HBSS−/−; Euroclone SpA, Italy). Lymphocytes were separated by 70%/30% discontinuous Percoll gradient (Cytiva; Marlborough, USA), washed in HBSS−/− and frozen in fetal bovine serum (FBS; Lonza, Basel, Switzerland) supplemented with 10% of DMSO (Lonza) in liquid nitrogen for further analysis.

Freshly isolated GBM tissue was dissociated by enzymatic digestion in gentleMACS Dissociator. Cells were then filtered through 100 μm cell strainer and washed in HBSS−/−. Lymphocytes were separated by 70%/30% discontinuous Percoll gradient, washed in HBSS−/−. and frozen in FBS with 10% of DMSO in liquid nitrogen.

Freshly isolated lung tissue was dissociated by mechanical disaggregation in gentleMACS Dissociator. Cells were then filtered through 70 μm cell strainer (Corning), washed with physiological saline solution (NaCl 0.9%; Baxter, Deerfield, USA) and frozen in FBS with 10% of DMSO in liquid nitrogen.

Human healthy thymus samples were obtained from children undergoing heart surgery for congenital heart diseases according to current clinical practice. Thymic tissue was cleaned from blood vessels and fat tissue, and cut in small pieces. Thymocytes were recovered through mechanical smashing and frozen in FBS with 10% of DMSO in liquid nitrogen.

Human leukemia cell line K562 (ATCC® CCL-243; Middlesex, UK), was cultured in Iscove's Modified Dulbecco's *medium* (IMDM; Euroclone SpA) supplemented with 10% FBS and 1% Penicillin-Streptomycin (P/S; Lonza). 721.221.G, human B-lymphoblastoid cell line transfected with HLA-E (221.G; kind gift from *Prof. M. Marcenaro*, University of Genoa, Italy) were cultured in Roswell Park Memorial Institute's medium (RPMI-1640; Euroclone SpA) supplemented with 10% FBS, 1% Pen/Strep/Amphotericin B (P/S/A; Lonza) and 1% Ultraglutamine (Lonza) (RPMI complete).

Human T cell leukemia cell line 1301 (sub-line of CCRF-CEM; Sigma Cat. No. 85112105) was cultured in RPMI-1640 supplemented with 10% FBS and 1% Ultraglutamine.

All cell lines were mycoplasma free. Mycoplasma test was performed on the P/S/A-free complete medium of 3-5 days cultured cells by PCR assay using following primers GPO-1 (5′-ACTCCTACGGGAGGCAGCAGT-3′) and MGSO (5′-TGCACCATCTGT CACTCTGTTAACCTC-3′).

METHOD DETAILS

Flow cytometry

For multiparametric flow cytometry analysis a standard staining protocol was used. Briefly, cells were first stained for live/dead discrimination by using Zombie Aqua fixable viability kit (BioLegend; San Diego, USA). Subsequently cells were washed with HBSS−/−. supplemented with 2% of FBS (FACS buffer) and incubated with the combination of anti-human monoclonal antibodies (mAbs), listed in the Key Resources Table, for 20 min in the dark at room temperature (RT), washed again and fixed in 1% paraformaldehyde (PFA; Santa Cruz Biotechnology, Dallas, USA).

Cytotoxicity of freshly isolated PBMCs was performed by a flow cytometry assay based on the measurement of the CD107a degranulation molecule (Aktas et al., 2009; Mikulak et al., 2019b; Roberto et al., 2018). Cells were plated in U-bottom 96-well plates (Corning) at a concentration of 10^6 cells/mL in RPMI complete supplemented with recombinant human (rh)IL-15 (10 ng/mL; Peprotech; Rocky Hill, USA). The day after, cells were cocultured or not with myelogenous leukemia K562 or B cell lymphoma 721.221.G (221.G) target cells, pre-stimulated or not overnight with Zoledronate (5 μM; Sigma Aldrich), at a ratio of E:T = 1:1. Anti-human CD107a mAb (clone H4A3; BD Biosciences) was added to the cell co-culture medium. After 4 hours of incubation at 37°C/5% CO_2 cells were collected, washed in HBSS−/− and stained for cellular membrane markers as described above. For masking experiments, PBMCs were incubated in the presence of anti-CD94 blocking mAb (Y9; kindly provided by *Prof. E. Marcenaro*) for 30 min at 37°C/5% CO_2. Subsequently CD107a cytotoxic assay was performed as described above.

To measure the cytotoxic effect of Vδ2 T cells, the death of K562 cells was measured by flow cytometry. After the co-culture of total PBMCs or flow cytometry-sorted $NKG2A^+$ and $NKG2A^-$ Vδ2 T cells with K562, cells were stained as described above. K562 cells were than identified based on physical parameters (Side Scatter Channel, SSC, versus Forward Scatter Channel, FSC) on singlets cells and dead cells were identified as the percentage (%) of positive for the live/dead Zombie/Aqua discrimination marker.

Intracellular cytokine concentration was measured by flow cytometry using anti-human IFN-γ mAb (clone B27), anti-human TNF-α mAb (clone Mab11) and anti-human IL-17A (clone BL168), all purchased from BioLegend. In specific, freshly isolated PBMCs were plated in U-bottom 96-well plates at a concentration of 10^6 cells/mL in RPMI complete supplemented with Zoledronate (5 μM) and rhIL-2 (200 U/mL; Peprotech). The day after, 1μg/mL of Golgi Plug, protein transport inhibitor (BD Biosciences) was added to the cell culture medium. After 4 hours at 37°C/5% CO_2 PBMCs were collected, washed with HBSS−/− and cellular membrane staining was performed as described above. Subsequently intracellular staining was done using Cytofix/Cytoperm™ kit (BD Biosciences) according to the manufacturer's instructions.

The analysis of telomere length was performed using a fluorescein-conjugated peptide nucleic acid (PNA) probe (Telomere PNA Kit/FITC for Flow Cytometry; Dako, Santa Clara, CA, USA), according to manufacturer's instructions. Briefly, thawed PBMCs were first stained with Zombie and anti-human CD3 (BV650), Vδ2 (BUV395) and NKG2A (BV711) mAbs (Key Resources Table), subsequently cell-surface protein crosslinking was performed using the BS^3 cross-linker (ThermoFisher Scientific, Waltham, MA, USA)

according to manufacturer's instructions. PBMCs were mixed with control 1301 cell line which display known long telomeres in ratio 1:1. The DNA was denatured for 10 min at 82°C either in hybridization solution without probe or containing fluorescein-conjugated PNA telomere probe. The hybridization took place in the dark at RT overnight followed by two washes with Hybridization Wash Buffer at 40°C. Propidium iodide staining was performed for the identification of $G_{0/1}$ cells. The relative telomere length (RTL) value was calculated as the ratio between the telomere signal of each sample and the control cells (1301 cell line) with correction for the DNA index of $G_{0/1}$ cells.

Apoptosis of PBMCs was measured by flow cytometry. Freshly isolated PBMCs were plated in U-bottom 96-well plates at a concentration of 10^6 cells/mL in RPMI complete supplemented with Zoledronate (5 μM) and rhIL-2 (200 U/mL). The day after cells were collected, washed with HBSS−/− and stained using the Annexin V-FITC Apoptosis Detection kit (Immunostep; Salamanca, Spain) according to manufacturer's instructions.

All samples were acquired by FACS Symphony A5 flow cytometer (BD Biosciences). Flow cytometry data were compensated by using single stained controls with BD Compbeads (BD Biosciences) conjugated to the specific fluorescent mAb. For accurate flow cytometry practice, all mAbs used for the study were previously titrated (Brummelman et al., 2018).

In vitro expansion of Vδ2 T cells

Vδ2 T cells were expanded from freshly isolated PBMCs as described (Kondo et al., 2011). In specific, PBMCs were plated in U-bottom 96-well plates at a concentration of 10^6 cells/mL in RPMI complete supplemented with Zoledronate (2.5 μM) and rhIL-2 (200 U/mL). Every 2 days, half of medium was replaced with the fresh rhIL-2 complete medium. Cells were collected after 5-8 days, washed with HBSS−/− and stained with Zombie Aqua fixable viability kit to discriminate dead cells and the appropriate mix of mAbs for 20 min in the dark at RT. Alternatively, cells were collected, washed with HBSS−/− and cytotoxicity was performed as described above.

In some experiments after 5-6 days of PBMCs culture we sorted as $NKG2A^+$ and $NKG2A^-$ Vδ2 T cell by FACS Melody cell sorter (BD Biosciences). After sorting cells were plated in U-bottom 96-well plates at a concentration of 0.5×10^6 cells/mL in RPMI complete with rhIL-2. After 5-6 days cells were collected, washed with HBSS−/− and stained for extracellular markers as described above.

Expansion of Vδ2 thymocytes was performed with thawed thymocytes plated at a concentration of 10^6 cells/mL in X-VIVO 15 serum-free hematopoietic cell medium (Lonza) with 5% human serum (Euroclone SpA), 1% P/S/A, 1% Ultraglutamine, 1% Na pyruvate (Lonza) and 1% NEAA (Lonza) and supplemented with Zoledronate (5 μM) and rhIL-2. Fresh rhIL-2 complete medium was added every 2 days. Cells were collected after 7 and 15 days, washed with HBSS−/− and stained for extracellular markers as described above. Intracellular detection of Ki-67 (clone B56; BD Biosciences) was performed by flow cytometry following fixation of cells with the intranuclear staining buffer set (eBioscience) according to manufacturer's instructions and by incubating with specific mAbs for 30 min at 4°C.

Single-cell RNA-seq and TCR-seq analysis

Single cell (sc)RNA-seq data were processed using the Seurat package (v. 3.1.1). The raw matrix counts generated by Pizzolato et al. (2019) were downloaded from GEO dataset GSE128223 (https://www.ncbi.nlm.nih.gov/geo/query/acc.cgi?acc=GSE128223) as indicated and imported in R (v. 3.6.1) as dataframes using the *read.table* function. These objects were subsequently used as input to generate Seurat objects (Stuart et al., 2019). Only cells with a number of RNA feature comprised between 200 and 2500, with less than 7500 counts/cell and less than 5% reads mapped to mitochondrial DNA were retained in the analysis. Cells originating from different experiments were integrated, generating a single Seurat object. After regressing-out cell cycle effects, Principal Component Analysis (PCA) was performed for initial dimensionality reduction. The *ElbowPlot* function was used to identify the eigenvectors to be retained in the downstream analyses. *t*-distributed stochastic neighbor embedding (*tSNE*) algorithm was run for further dimensionality reduction, using the first 20 PCA components as input, corresponding to > 90% explained variance. Clusters were identified using the *FindNeighbors* and *FindClusters* algorithms using the first two dimensions of the tSNE. Expression levels of genes of interest (GOI) were plotted at single-cell resolution using the *FeaturePlot* function. Violin Plots were generated with *VlnPlot* and heatmaps using the *DoHeatmap* function. Differentially expressed genes across clusters were identified using the *FindAllMArkers* function and top 2000 variable genes at global scale were selected using the *FindVariableFeatures* function. Volcano plots show differentially expressed genes (DEGs) with evidenced genes in red circles as significant *adj. P value* < 0.05 and Log_2-FoldChange differential expression > 0.25.

The pseudotime analysis was generated using Stream (Chen et al., 2019). Count data were initially log-normalized and then used as input to call the stream function. Cluster colors were superimposed by using the –l/-c parameters and by feeding the stream function with the clusters previously identified by Seurat. Expression-weighted 2D kernel density plots were generated with the Nebulosa package (v. 1.0.0) using Kernel discrimination analysis function (kda).

Paired scRNA-seq and scTCR-seq dataset of γδ T cells from PB (n = *2*, GEO: GSE149356) were acquired as described (Tan et al., 2020), Vδ2 T cells were selected then queried according to normalized and scaled *KLRC1* expression. TCR frequencies were calculated by the absolute copy number of CDR3 amino sequence. Data were analyzed by Seurat package in R.

Gene editing of PB γδ T cells

To edit the target gene, freshly isolated human PBMCs from HDs selected for high (> 70%) expression of NKG2A on Vδ2 T cells were plated at a concentration of $4x10^6$ cells/mL in RPMI complete supplemented with Zoledronate (2.5 μM) and rhIL-2 (200 U/mL) for

2 days. Alt-R® CRISPR-Cas9 crRNAs (crRNAs) targeting the human *KLRC1* gene (ID gRNA: Hs.Cas9.KLRC1.1.AA) and negative control (Cat. N. 1072544) crRNA were synthesized by Integrated DNA Technologies (IDT; Coralville, IA, USA). Guide RNAs (gRNAs) duplex were generated by incubating equimolar concentrations of crRNAs targeting *KLRC1* or control with Alt-R® CRIPSR-Cas9 tracrRNA ATTO^{TM} 550 (IDT; Cat. N.1075928) in IDTE buffer according to the manufacturer's instructions, at 95°C for 5 minutes. Reactions were cooled to RT, followed by addition of Alt-R® S.p. HiFi Cas9 Nuclease V3 (IDT). The Cas9 protein and gRNA mixture was next incubated at RT for 15 minutes to form ribonucleoprotein complexes (RNP). Alt-R® Cas9 Electroporation Enhancer (IDT) was added to the RNP complexes before performing the nucleofection. 40x10^6 of Zoledronate-stimulated PBMCs were collected, washed 5 times with HBSS−/− and resuspended in 80 μL of Human T Nucleofector solution (Lonza). Next, cells were electroporated with 24 μL of RNP in a cuvette using a Nucleofector^{TM} 2D device (Lonza) with program T cells Human Stimul, T-023. Electroporated cells were then plated in U-bottom 96-well plates at a concentration of 10^6 cells/mL in RPMI complete supplemented with rhIL-2 (200 U/mL). Every 2 days, half of medium was replaced with the fresh rhIL-2 complete medium. After 4 days, cytotoxicity against 221.G target cells was performed as described above.

Clinical outcome analysis

Gene Expression Profiling Interactive Analysis 2 (GEPIA2; http://gepia2.cancer-pku.cn/#index) is an open-access dataset for analyzing RNA sequencing expression data from tumors and normal samples from The Cancer Genome Atlas (TCGA; https://www.cancer.gov/tcga/) and the Genotype-Tissue Expression project (GTEx; https://www.gtexportal.org/home/index.html). GEPIA2 was used to assess survival of TCGA patients with GBM, lung adenocarcinoma (NSCLC) and HCC. Both gene correlation analysis between expression of *KLRC1* and *TRDV2*, a surrogate of Vδ2 T cells, and tumor/normal differential *HLA-E* gene expression were performed with GEPIA2. GEPIA2 was used to assess survival of TCGA patients with GBM, NSCLC and HCC. The cox proportional hazard ratio (HR) of the *Vδ2 T-SI* high and low-expression cohort was calculated by GEPIA2, while 95% CI was calculated as "exp [ln(HR)± z*SE], with SE standard error" (Tierney et al., 2007).

QUANTIFICATION AND STATISTICAL ANALYSIS

Analysis was performed using GraphPad Prism version 7. For the comparison of 2 groups of samples *t test* or *Kolmogorov-Smirnov* test were applied. Experiments with more than 2 groups were analyzed by *ANOVA* test with *Tukey's* comparison test. When specified, Pearson's rank correlations analysis was used. The data are depicted as vertical bars or one square corresponding to mean value ± estimated standard error (SEM) with aligned dots or as scattered plots of paired observations. For some experiments pie charts with the mean value ± SEM were used. All statistical details of the experiments, including the statistical tests used and the number of subjects analyzed, are reported in each figure legend. Statistically significant *P values* were represented with GraphPad (GP) style and summarized with following number of asterisks (*): *P<0.05; **P<0.01; ***P<0.001; ****P<0.0001. All flow cytometry data, comprising the *t-SNE* algorithm, were analyzed by FlowJo software version 9.9.6 (FlowJo LLC; Ashland, USA).

Graphical abstract was prepared in Biorender.com (Toronto, Canada).